UCLA
UCLA Electronic Theses and Dissertations

Title

Innovative Approaches to Electrochemical Energy Storage: Advancements in Microelectrodes and Vanadium Oxide Cathodes

Permalink

https://escholarship.org/uc/item/62d6h0xf

Author

Xie, Zhangdi

Publication Date

2024

Peer reviewed|Thesis/dissertation

eScholarship.org Powered by the California Digital Library
University of California

UNIVERSITY OF CALIFORNIA

Los Angeles

Innovative Approaches to Electrochemical Energy Storage: Advancements in Microelectrodes and Vanadium Oxide Cathodes

A thesis submitted in partial satisfaction

of the requirements for the degree Master of Science

in Chemical Engineering

by

Zhangdi Xie

2024

© Copyright by

Zhangdi Xie

2024

ABSTRACT OF THE THESIS

Innovative Approaches to Electrochemical Energy Storage: Advancements in Microelectrodes and Vanadium Oxide Cathodes

by

Zhangdi Xie

Master of Science in Chemical Engineering

University of California, Los Angeles, 2024

Professor Yuzhang Li, Chair

Electrochemical energy storage plays a vital role in facilitating the integration of renewable energy sources, improving the efficiency of portable electronic gadgets and electric vehicles. This thesis explores innovative advancements in electrochemical energy storage, focusing on two main areas: microelectrodes and vanadium oxide cathodes. The first chapter elaborates on the distinctive features and manufacturing techniques of microelectrode needles and arrays, highlighting their

exceptional accuracy in tackling unresolved scientific questions in energy storage. By enabling ultrafast electrodeposition kinetics and localized electrochemical measurements, they provide critical insights into the behavior of various energy storage materials, demonstrating their potential to challenge the initial understanding of fundamental energy storage mechanism. Future opportunities in electrodeposition morphology, in situ characterization and high-throughput experimenting have been identified, to further advance microelectrode technology.

The second chapter delves into the structural and electrochemical advantages of vanadium oxide cathodes for aqueous zinc ion batteries (AZIBs). These cathodes are pivotal due to their potential for high energy density and extended cycle life, addressing critical obstacles in existing energy storage systems. AZIBs, equipped with their ecologically sound aqueous electrolytes, present safer options compared to lithium-ion batteries (LIBs), rendering them appropriate for extensive energy storage purposes. The chapter discusses innovative strategies to overcome current constrains, including the development of laser-scribed VO_x-rGO heterostructures that exhibits exceptional pseudocapacitive Zn^{2+} storage and remarkable electrochemical performance. This research not only improves the calendar life of AZIBs, but also paves the way for future progress in cathodic engineering, electrolyte chemistry, and large-scale implementation. By enhancing the efficiency and durability of energy storage systems, these research topics have significant implications for supporting the global transition to cleaner energy solutions.

The thesis of Zhangdi Xie is approved.

Richard B. Kaner

Carlos Gilberto Morales Guio

Yuzhang Li, Committee Chair

University of California, Los Angeles

2024

Table of Contents

Chapter 1: Microelectrodes for Electrochemical Energy Storage 1

1.1 Introduction 1
1.2 Key Features and Advantages of Microelectrodes 2
1.3 Fabrication of Microelectrodes 5
1.3.1 Microelectrode Needles 5
1.3.2 Microelectrode Arrays 6
1.4 Recent Advances and Applications of Microelectrodes 8
1.4.1 Ultrafast Electrodeposition of Lithium Metal 8
1.4.2 Characterization of Intercalation Materials 10
1.5 Future Opportunities 13

Chapter 2: Vanadium Oxide Cathodes for Aqueous Zinc Ion Batteries 18

2.1 Introduction 18
2.2 Understanding of Structural Superiorities of Vanadium Oxide Cathodes 20
2.3 Current Challenges with Vanadium Oxide Cathodes in AZIBs 21
2.4 Enhancing Electrochemical Performance of Vanadium Oxide Cathodes 23
2.4.1 Mixed Valence States of Vanadium 23
2.4.2 Heterostructures/Composite Structures with Conducting Additives 25
2.5 Laser-Scribed VO_x-rGO Heterostructure for Ultrafast Zinc-Ion Energy Storage 25
2.5.1 Synthesis method 26
2.5.2 Materials characterization 27
2.5.3 Pseudocapacitive Zn^{2+} storage 29
2.5.4 Electrochemical performance 33
2.5.5 Calendar life and anti-aging ability 35
2.6 Future opportunities 39
2.6.1 Cathodic engineering 39
2.6.2 Electrolyte chemistry 41
2.6.3 Large-Scale and Practical Applications 42

Reference 44

Table of Figures

Figure 1.Reduction of the electrode size from macro to micro-scale. 2
(a) The mass transport on macrodisk and microdisk electrode (macrodisk: semi-infinite linear diffusion; microdisk: radial diffusion).
(b) The cyclic voltammogram (CV) profile of macrodisk and microdisk electrode (macrodisk: peak-shaped; microdisk: sigmoidal-shaped).

Figure 2. Typical configurations of microelectrodes. 7
(a) Micro-needle electrode is manufactured by a tungsten or platinum needle coated with glass or a polymer, to get a constant exposure of electrochemically-active area.
(b) Microfabrication approaches can create an array of microelectrodes on a single substrate, with tens of or more single particles attached.

Figure 3. Ultrafast electrodeposition of Li metal. 10
(a-c) High-resolution cryo-EM image and SAED pattern of Li column morphology at low current density. (d-f) High-resolution cryo-EM image and SAED pattern of faceted rhombic dodecahedron Li particle at ultrafast current density.

Figure 4. Characterization of intercalation materials with microelectrodes. 13
(a) Constant current cycling of a single $LiFePO_4$ particle to show charge and discharge rates as high as 750 C-rate (~5 seconds).
(b) Electrochemical impedance spectroscopy (EIS) conducted on a single $LiCoO_2$ over time.
(c-d) Potentiostatic intermittent titration technique (PITT) to reveal that the diffusion time is independent of the diameters of NMC secondary particles.

Figure 5. Electrodeposition of reactive metals and quantitative analysis of electrolyte kinetics with microelectrodes. 15
(a) The morphologies of various polymorphs, consisting solely of a family of close-packed planes.
(b) Scheme for morphological transition of deposited Li, which is dictated by relative kinetics between Li deposition rate and SEI formation rate.
(c) Quantitative analysis of electrolyte kinetics to correlate transition current density with Li morphology.

Figure 6. Characterization techniques at multiple length scales (red dotted circle: microelectrode measurements). 17

Figure 7. Materials characterization of the laser-scribed VOx-rGO heterostructure 29
(a) SEM image of the VO_x-rGO heterostructure showing highly exposed rGO sheets with nano-VO_x particles uniformly embedded in the porous structure.
(b) EDS spectra before and after calcination, indicating the removal of chlorine and conversion of V^{3+} to higher oxidation states.
(c) SEM image of commercial V_2O_5, showing bulky vanadium species with significant aggregation.

(d) XRD patterns of the final VO_x-rGO heterostructure, illustrating the presence of orthorhombic V_2O_5 and monoclinic VO_2 phases.

Figure 8. Pseudocapacitive Zn2+ storage of the laser-scribed VOx-rGO heterostructure.. 32
(a) Cyclic voltammetry (CV) curves recorded in the voltage range of 0.3 to 1.6 V, displaying two pairs of redox peaks indicative of reversible Faradaic reactions.
(b) Plot of log(i) vs. log(v) for the four redox peaks, showing b values close to 1, suggesting predominantly surface-controlled capacitive processes.
(c) Bar graph depicting the contributions of surface-controlled and diffusion-controlled processes to the total capacity at various scan rates. The proportion of surface-controlled charge storage increases with increasing scan rates, reaching 98% at 2 mV s^{-1}.
(d) Zn^{2+} diffusion coefficients calculated from GITT curves, showing high diffusion kinetics of VO_x-rGO heterostructure, especially below 0.9 V.

Figure 9. Electrochemical performance of the laser-scribed VOx-rGO heterostructure 35
(a) Voltage vs. capacity profile at 0.2 A g^{-1}, showing the high specific capacity (~505 mAh g^{-1}) of VOx-rGO compared to commercial V_2O_5.
(b) Areal capacity retention of VOx-rGO from low to high current densities (0.5 to 100 A g^{-1}), maintaining 74% capacity at 100 A g^{-1} for a 0.8 mg cm^{-2} loading.
(c) Specific capacity of VOx-rGO at high current densities (50 to 100 A g^{-1}), demonstrating a stable capacity around 220 mAh g^{-1} over multiple cycles.
(d) Long-term cycling stability and Coulombic efficiency (CE) of VOx-rGO at 30 A g^{-1}, with 97.2% capacity retention after 1000 cycles and an average CE of 99.97%.

Figure 10. Calendar life and anti-aging ability of the laser-scribed VOx-rGO heterostructure 38
(a) CE_{aging} of ZIBs at different states of charge (SOC) over 120 hours, showing significant CE loss at 100% SOC, and over 100% of capacity preserved at 50% and 30% SOC.
(b) Comparison of CE_{aging} between 2m $ZnSO_4$ in H_2O and D_2O, with a table summarizing Zn^{2+} insertion capacity loss over time.
(c) CE_{aging} after 24 hours for different electrolyte compositions, highlighting the benefits of D_2O and PVA hydrogel.
(d) CE_{aging} over time for initial and triple dosage of cathode precursors, indicating the potential for large-scale applications.

Acknowledgement

Many sincere thanks to:

My supervisor and committee chair, Prof. Yuzhang Li, for his valuable guidance and inspiration on my research.

My cooperation and supervisor committee, Prof. Richard Kaner, for his unreserved support in our joint research project.

My committee, Prof. Carlos Morales-Guio for his time in reviewing this work.

Haoyang Wu, for working together in the field of aqueous batteries; Bo Liu and Jin Koo Kim, for their inspiring advice in my research; and all Li group members, for being trusted colleagues and promoting the growth of our group.

Gray Carson, Bradley Kroes, Sophia Uemura, for their commitment in our research collaboration; Yuto Katsuyama; Zhiyin Yang, for their participation in our joint meetings; and all Kaner group members for their openness in sharing me with lab recourses.

Li Shen and Qingyang Yin, for their accommodating with my usage of Lu lab equipment.

Xinyue Zhang and Qian Liu, for being close friends and all wonderful time we spend together, and all friends I met during my stay at UCLA for enriching my life here.

Also the emotional support from my parents, Naxin Xie and Ling Zhang.

Chapter 1: Microelectrodes for Electrochemical Energy Storage

1.1 Introduction

Electrochemical energy storage is a critically important technology towards the transition to a clean and renewable energy future. Such systems are developed based on the electrochemical redox of solution- and/or solid species. Owing to differences in the electrochemical potential, these redox reactions enable energy to be stored and delivered for practical purposes, with applications in electric vehicles, grid storage, and beyond.

Advanced understanding of electrochemical systems requires precise measurements of the currents and voltages in electrochemical reactions. For energy storage materials, such measurements are conducted on macroscopic porous electrodes containing a current collector, redox-active materials, as well as conductive additives and binders.[1] These porous electrodes are featured with high electrochemical surface area for high power density and efficient packing of redox-active species for high energy density, making them advantageous for commercial energy storage demands.

Although macroscopic porous electrodes are widely used and simple to construct, their inherent heterogeneity makes it very difficult to understand the intrinsic behavior of energy storage materials.[2] An alternate strategy is microelectrode, also called ultramicroelectrode (UME). Microelectrodes are electrodes with one or more dimensions small enough, hence the properties at the electrode-electrolyte interface are functionalized by size. These microelectrodes, invented in the early 1980s, have long been utilized in electrochemical systems to empower shorter mass transport distances, shorter diffusion times, and higher current densities.[3, 4] They also enable

localized measurements of electrochemical currents and voltages, thus are applicable in a variety of electrochemical systems including electrocatalysts,[5] sensing[6] and neurotransmitters.[7]

In this chapter, the key features and advantages of microelectrode electrochemistry are fully elaborated and correlate to its application to electrochemical energy storage. Fabrication methods for both microelectrode needles and arrays are introduced accordingly to secure accurate measurements to answer unsolved scientific questions in energy storage. Inspired by current advancements in this field, future opportunities for microelectrodes are outlined conclusively.

1.2 Key Features and Advantages of Microelectrodes

The key defining feature of microelectrode electrochemistry is the reduction of the electrode size from macroscopic (>5 mm) to microscopic (<100 micron) dimensions. This size reduction induces significant difference in the diffusion pathway of electroactive species from the bulk electrolyte to the electrode-electrolyte interface (Figure 1a). The key advantages induced by microstructure and corresponding enhancement in diffusion are summarized in this section.

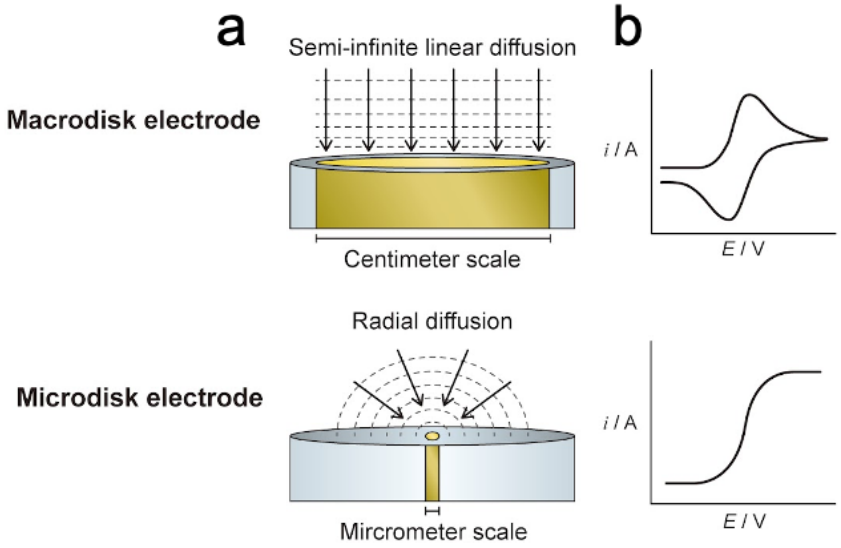


Figure 1. Reduction of the electrode size from macro to micro-scale.

(a) The mass transport on macrodisk and microdisk electrode (macrodisk: semi-infinite linear diffusion; microdisk: radial diffusion).

(b) The cyclic voltammogram (CV) profile of macrodisk and microdisk electrode (macrodisk: peak-shaped; microdisk: sigmoidal-shaped).

(1) Enhanced Mass Transport

The small dimensions of microelectrodes significantly improve mass transport to the electrode surface. This improvement reduces concentration polarization, which is a common issue in larger electrodes that can limit performance.[8] Enhanced mass transport allows for higher deposition rates and improved efficiency in energy storage systems. A micron-sized single particle can be attached to microelectrodes as a host material, facilitating faster and more uniform ion intercalation for fundamental study.

(2) Reduced Diffusion Layer Thickness

Microelectrodes have much thinner diffusion layers compared to larger electrodes. This decrease in diffusion layer thickness is advantageous because it helps accelerate the attainment of steady-state conditions, which is essential for the realization of higher current densities and faster kinetics.[9] This is especially beneficial for conversion-type electrodes, such as those used in lithium-sulfur or lithium-air batteries, where microelectrodes play a crucial role in efficient redox reactions by facilitating the rapid transport of reactants and products across the electrode surface.

(3) Minimized Ohmic Drop and double-layer capacitance

Microelectrodes minimize the ohmic drop due to their reduced size, leading to more accurate control over the applied potential and current during electrochemical processes.[10] Depending on the system of interest, this is necessary for rigorous electrochemical measurements or to control the deposition of active materials, which is a critical step in designing high-performance energy storage systems.

From macroelectrodes to disk-shaped microneedles, the double-layer capacitance (DLC) is credibly reduced. This enables a rapid change in the electrode potential, which can be reflected by the voltammetric measurement in a sub-microsecond time scale. Different from typical voltammogram of macroelectrodes, a well-defined sigmoidal shape is expected for microelectrodes (Figure 1b), and the limiting plateau current from CV analysis is defined by

$$i_{T\infty} = 4nFC_0\,Dr$$

where i is the steady-state limiting current (A), F is Faraday constant (96500 C), and r is electrode radius (cm). The size of microelectrode is determined from the limiting current measured from steady-state voltammogram in a sigmoidal shape (with known C_0 and D_r values).[11]

(4) Localized Deposition

Microelectrodes enable highly localized deposition, which is imperative for morphological and structural control of the deposited material at a micron scale. Particularly when applied to micro-batteries and micro-supercapacitors, selective deposition can promote the creation of patterned electrodes with large surface area and optimized geometries for improved longevity of the battery.[12, 13] Localized control is also important for the architectural diversity of advanced

nanostructures, where fabricating micro-textures on nanomaterials can lead to unique properties of electrode materials.[14]

Microelectrodes offers many compelling advantages including increased mass transport, reduced thickness of the diffusion layer, minimized ohmic drop, and selectively deposition of nanomaterials. These capabilities make them invaluable tools for multiple energy storage applications. In the next section, we will introduce the fabrication and characterization of microelectrodes, which secure their appropriate utility and impact in advancing battery technologies.

1.3 Fabrication of Microelectrodes

There have been two primary methods to fabricate microelectrodes. The first method is to use a sharp metallic needle that is only several tens of micrometers sharp at the tip. These needles are often made of tungsten/platinum and can be integrated into standard two- and three-electrode electrochemical experiments. The second method is newly developed from semiconductor processing to fabricate microelectrode arrays.

1.3.1 Microelectrode Needles

Tungsten or platinum wires as small as <1 micron can be purchased from different commercial vendors. One end of the microwire is fastened with a thin copper wire externally for electrical contact. The walls of tungsten or platinum wires are typically encapsulated by glass capillary tube and epoxy resin such that only the “tip” of the needle is exposed to the electrolyte (Figure 2a). Because of its perfect insulation, inertness, and transparency, glass is the ideal material to insert metallic wires in. In contemporary scientific glass blowing, perfect metal-to-glass sealing

is expected to secure the exposed electrochemically-active area. To avoid air trapping between the fine capillary jet and metal contact, the sealing must be done gradually from one end to the other, which typically necessitates a postmortem under an optical microscope. Grinding papers will next be used to remove any imperfectly sealed areas that include air bubbles, and the top of the tip will be polished to reveal the conductive metal disk.[15] After that, the cyclic voltammetry can be performed in a solution with redox mediators (ie. $[Fe(CN)_6]^{3-}$, $[Fe(CN)_6]^{4-}$ in aqueous media and $Fe(C_5H_5)^2$, $Fe(C_2H_5)^{2+}$ in organic solvents) to characterize the quality of as-made electrode.[16]

1.3.2 Microelectrode Arrays

A more recent approach is to use microfabricated microelectrode arrays developed by semiconductor manufacturing.[17] (Figure 2b) Optical photolithography techniques are used to pattern metallic microelectrodes like Au or Al on a substrate,[18] typically silicon or silicon oxide due to its widespread use in microelectronics. Millimeter-sized contacts, or pads, are constructed at the edge of the chips in connection to the potentiostat, with smaller interconnects connecting the pads to the microelectrodes. The wires are typically passivated with an insulating material like silicon nitride, silicon oxide, or polyimide, while the microelectrodes are exposed using lithography and reactive ion etch. For redox flow or electrodeposition, microelectrodes are functionalized as the working electrodes.[19] For ion insertion reactions involving a solid, particles would need to be manually assembled onto the microelectrodes.[20] Finally, a liquid electrolyte is used to ionically connect the microelectrodes to the counter-electrodes, thereby completing the electrochemical circuit.

The microfabricated microelectrode arrays have significant advantages of compact design, clean-room-based automatic manufacturing, high channel counts and densities. Many university

clean rooms can define <5 micron features using contact mask aligner lithography. Even smaller features can be constructed using projection lithography (~500 nm), direct write (~300 nm), or electron beam lithography (~50 nm). Moreover, microfabricated microelectrode arrays implement the definition of tens, hundreds, or even thousands of individually addressable microelectrodes on a single chip. By multiplexing these measurements, a single chip provides the opportunity for high-throughput and potentially automated experiments. One recent example is the Electrolab, an autonomous testbed for the study of redox flow molecules using microfabricated electrodes[18].

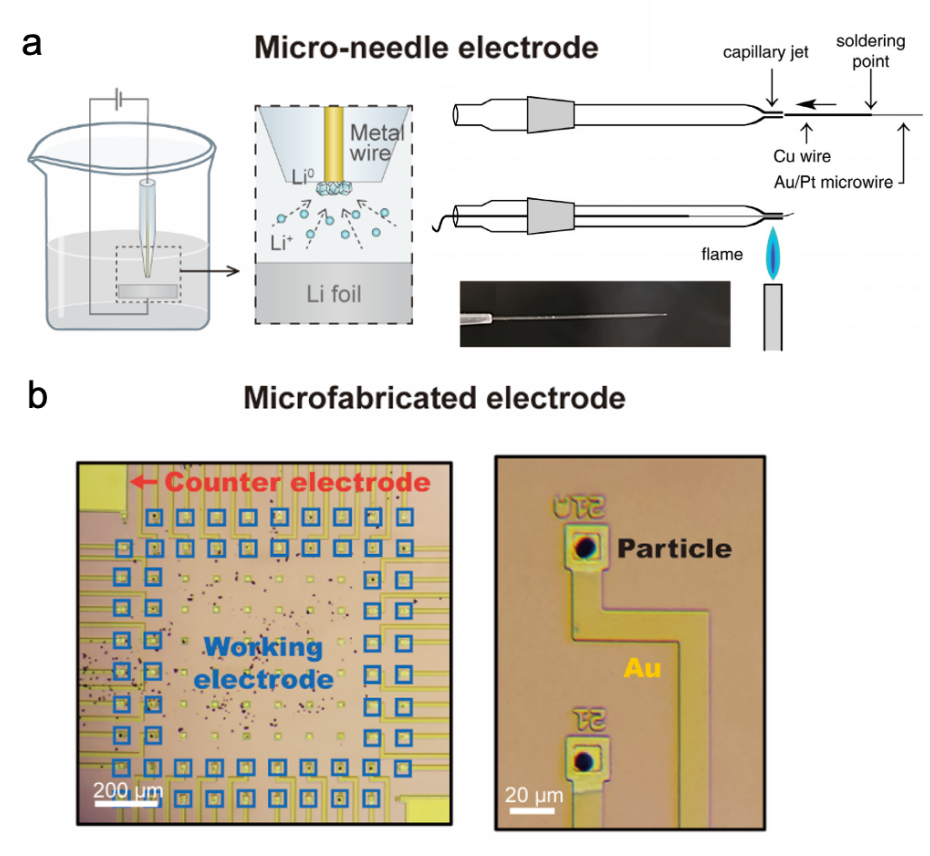


Figure 2. Typical configurations of microelectrodes.

(a) Micro-needle electrode is manufactured by a tungsten or platinum needle coated with glass or a polymer, to get a constant exposure of electrochemically-active area.[15] Copyright 2012, ACS Publications.

(b) Microfabrication approaches can create an array of microelectrodes on a single substrate, with tens of or more single particles attached.[20] Copyright 2023, Royal Society of Chemistry.

1.4 Recent Advances and Applications of Microelectrodes

This section has a particular focus on recent advances and applications of microelectrodes, including the ultrafast electrodeposition of lithium (Li) metals and characterization of intercalation materials. The small size of microelectrodes leads to enhanced mass transport and reduced diffusion layer thickness, enabling ultrafast electrodeposition rates and more precise control over the deposition process. Additionally, microelectrodes have emerged as powerful tools for probing the intercalation of metal ions in electrochemical energy storage systems. These miniature electrodes facilitate single-particle electrochemical experiments, providing insights into the fundamental processes governing ion intercalation in various anode and cathode materials, particularly in LIBs and lithium metal batteries (LMBs).

1.4.1 Ultrafast Electrodeposition of Lithium Metal

Electrodeposition of Li metal is exclusive for developing high-energy batteries. However, the concurrent formation of the solid electrolyte interphase (SEI) complicates this process. The SEI forms immediately upon contact of Li metal with the electrolyte, affecting the deposition morphology and complicating our understanding of Li electrodeposition.

Yuan et al. have recently made notable progress in decoupling Li deposition from SEI growth by utilizing UME geometries.[21] At extremely high current densities, they noticed that various lithium deposits in model electrolytes transform into a distinct and well-defined polyhedron with flat facets. This finding is unexpected, as it contradicts earlier research that shown

Li dendrites become more complex at greater current densities (Figure 3). The morphology of this structure was recognized as a rhombic dodecahedron by cryo-EM technique. This matches the theoretical Wulff structure prediction for a body-centered cubic (BCC) crystal when there is no passivation film present.

Yuan's findings questioned the established beliefs that high current densities encourage the griwth of dendritic Li and that the shape of Li deposition is controlled by electrolyte chemistry. These UME tests have shown that the inherent shape of Li metal is a non-dendritic rhombic dodecahedron, regardless of the electrolyte chemistry and current collector substrate. This discovery demonstrates that by surpassing the formation of solid-electrolyte interphase (SEI), the impact of these factors on the shape of lithium deposition may be eliminated. This provides valuable knowledge on how to prevent critical failure modes while rapidly charging lithium metal batteries (LMBs).

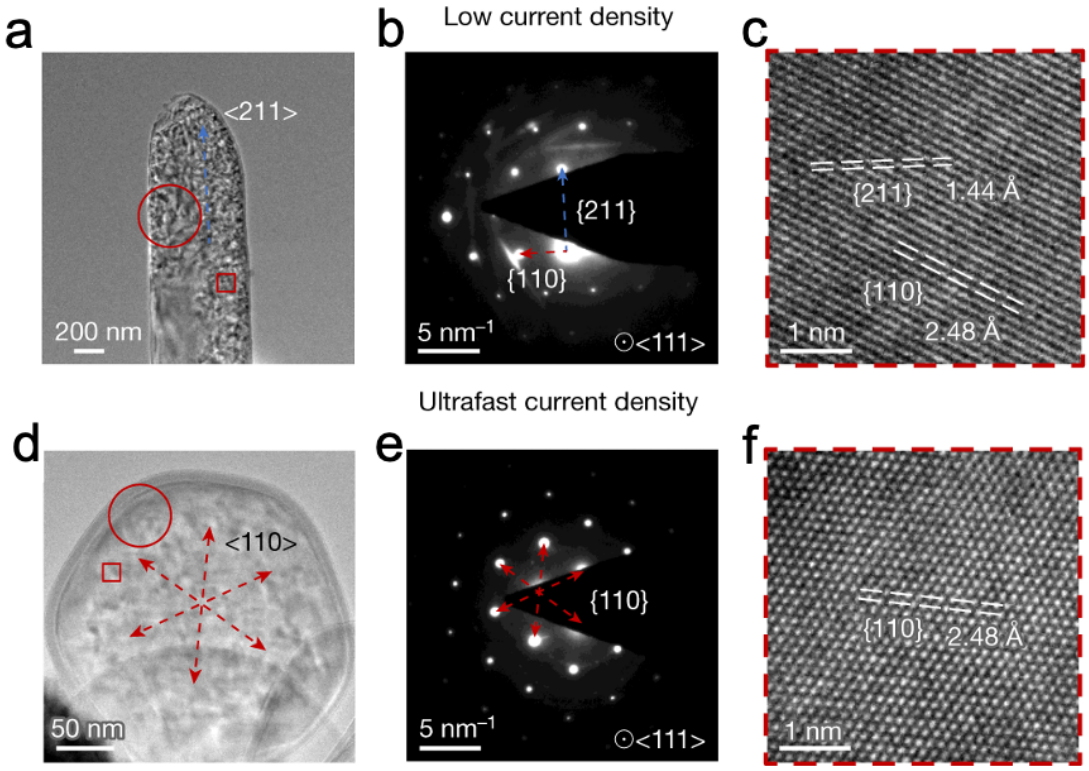


Figure 3. Ultrafast electrodeposition of Li metal.

(a-c) High-resolution cryo-EM image and SAED pattern of Li column morphology at low current density. (d-f) High-resolution cryo-EM image and SAED pattern of faceted rhombic dodecahedron Li particle at ultrafast current density.[21] Copyright 2023, Springer Nature Limited.

1.4.2 Characterization of Intercalation Materials

(1) Quantifying Kinetics of Intercalation

Microelectrodes have been instrumental in determining the ultimate rate capabilities of intercalation materials. The rapid mass transfer in electrolytes is made possible by the small dimensions of microelectrodes, allowing for high-speed performance. Through the analysis of individual cathode particle, scientists have successfully expanded the limits of how quickly charges may be stored and released, creating exceptionally rapid reactions that are challenging to achieve with conventional cathode materials. For instance, the use of microelectrodes in single-particle experiments has shown that charge and discharge rates can reach up to 750C, equivalent to discharging in around 10 seconds, in a single $LiFePO_4$ particle (Figure 4a).[22] Furthermore, the study conducted by Dokko et al. has revealed that microelectrodes have the ability to investigate rapid intercalation processes, as evidenced by the reported ultra-fast speeds of up to 1000C in single graphite particles.[23]

(2) Identifying Reaction and Diffusion Coefficients

Microelectrodes have also been widely employed to quantify the reactivity and diffusion characteristics of metal ion intercalation. Commonly used techniques include electrochemical impedance spectroscopy (EIS), potentiostatic intermittent titration technique (PITT), and quasi-Tafel analysis. These techniques enable researchers to ascertain crucial parameters such as the exchange current density (j_0) and the diffusivity (D) of ions within solid electrodes.

Electrochemical Impedance Spectroscopy (EIS) is a technique that analyzes the impedance of an electrode across a variety of frequencies. It provides valuable information on the resistance to charge transfer and the diffusion of ions. Microelectrodes with precise geometries are very suitable for EIS studies, as they provide dependable data that are applicable in continuous physical models. Dokko et al. reported a series of EIS study in Li^+ insertion into the single particle electrodes, where the chemical diffusion coefficient, charge transfer resistances and SEI-induced properties were fully investigated (Figure 4b).[24-26]

The Potentiostatic Intermittent Titration Technique (PITT) applies a constant potential and measures the ensuing current to determine the diffusion coefficients. Due to the small size of microelectrodes, the effects of particle size distribution and the presence of additives and binders are minimized, resulting in more accurate results. In a significant study conducted by Min et al., a microfabricated microelectrode array was utilized to measure reaction and diffusion characteristics across a total of 21 particles (Figure 4c-d). Their research revealed that smaller particles displayed comparable diffusion and response time constants to larger particles, which can be explained by the occurrence of particle breakage and subsequent penetration of electrolyte. This study emphasized a statistical methodology to examine numerous single-particle electrochemistry datasets, aiding in the advancement of models that integrate the impacts of electrolyte penetration.

Quasi-Tafel Analysis is another method that involves examining the current-voltage characteristics in order to calculate exchange current densities. This allows for a better understanding of the kinetics of intercalation reactions. To summarize, microelectrodes are considered the most reliable method for investigating the insertion of metal ions. They provide exceptional accuracy in determining reaction and diffusion coefficients, as well as studying the intercalation kinetics at the individual particle level. The knowledge acquired from these investigations is significant for furthering the comprehension of electrochemical energy storage and improving the efficiency of batteries.

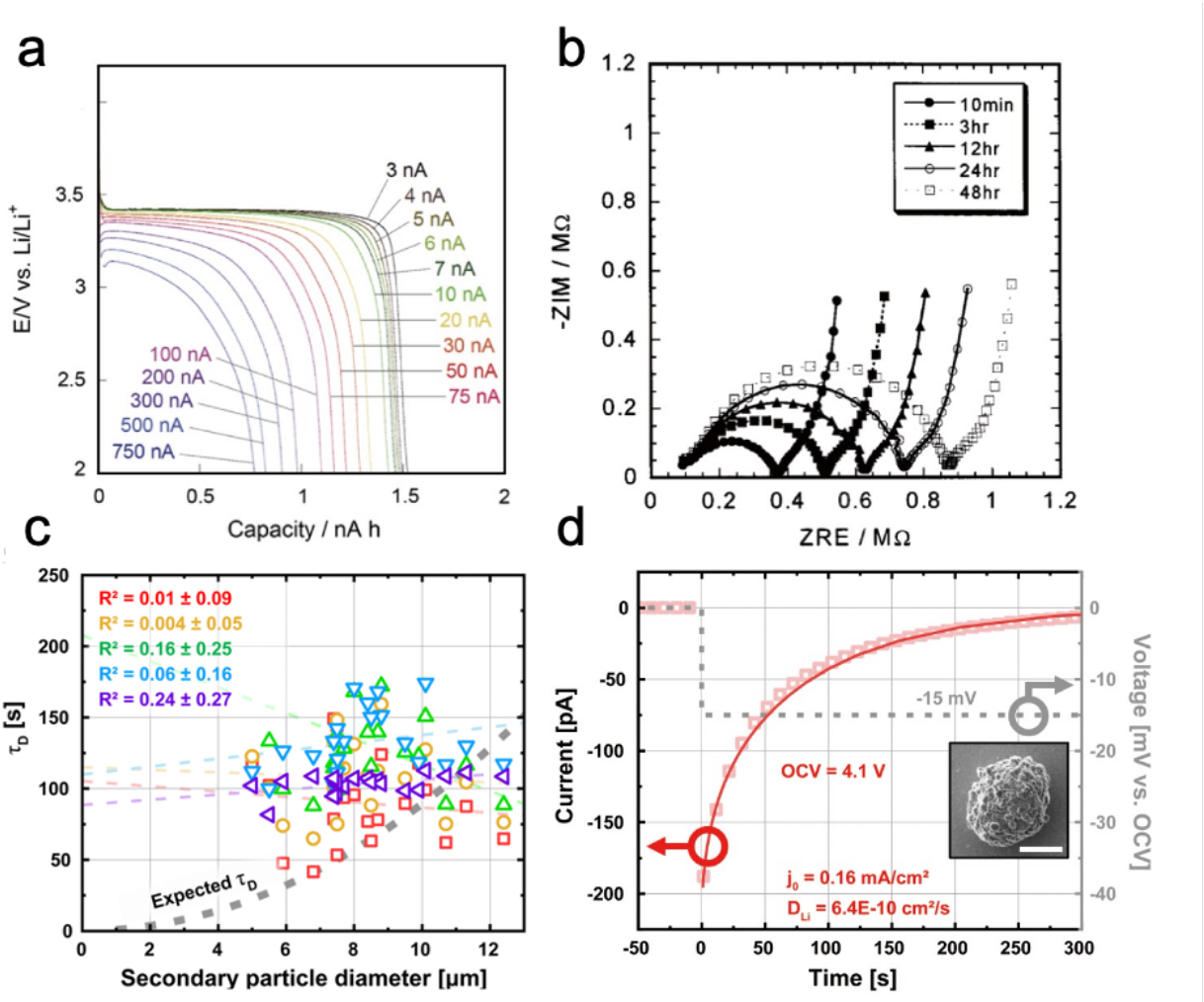


Figure 4. Characterization of intercalation materials with microelectrodes.
(a) Constant current cycling of a single $LiFePO_4$ particle to show charge and discharge rates as high as 750 C-rate (~5 seconds).[22] Copyright 2012, Elsevier B.V. (b) Electrochemical impedance spectroscopy (EIS) conducted on a single $LiCoO_2$ over time.[26] Copyright 2001, IOP Publishing (c-d) Potentiostatic intermittent titration technique (PITT) to reveal that the diffusion time is independent of the diameters of NMC secondary particles.[20] Copyright 2023, Royal Society of Chemistry.

1.5 Future Opportunities

The realm of microelectrode applications in electrochemical energy storage and conversion is on the verge of substantial progress. Recent advancements have showcased the adaptability and accuracy of microelectrodes in examining essential activities at the micro- to nano-scale, facilitating thorough examinations of electrochemical phenomena. As we consider the future, there are multiple potential chances to increase the utilization of microelectrodes. These include manipulating the electrodeposition of reactive metals beyond Li, improving our comprehension of electrolyte kinetics, and facilitating high-throughput experimentation.

(1) Electrodeposition of Other Reactive Metals

Beyond Li, microelectrodes may be used to manipulate the deposition morphologies of various reactive metals, which could have a significant impact on future technologies by decoupling them from SEI influence. As illustrated in Figure 5a, the stability of metal morphologies is usually determined by their crystallographic orientations. Metals like sodium (Na),

and potassium (K) exhibit the rhombic dodecahedron as their most stable morphology, while aluminum (Al) and calcium (Ca) favor the octahedral structure. Hexagonal-close packed (HCP) metals, on the other hand, tend to form plate-like hexagonal columns with a high aspect ratio to minimize total surface energy. These insights open up a wide range of possibilities to transform the most stable polymorphs on microelectrodes and enhance the reversibility of metal ion electrodeposition.

(2) Quantitative Analysis of Electrolyte Kinetics

Microelectrodes provide a powerful platform to bridge morphological transitions and electrolyte chemistry. When the applied current density exceeds a critical threshold, the rate of metal deposition outpaces SEI formation, leading to a morphological transition as depicted in Figure 5b. Since electrolyte chemistry influences both Li deposition kinetics and SEI formation, the current density required to decouple these processes will vary with different electrolyte formulations. By measuring transition current densities across various electrolytes, researchers can quantify electrolyte decomposition kinetics and distinguish between electrochemical electrolyte decomposition and spontaneous corrosion of Li (Figure 5c). This method can guide the development of new electrolytes and SEI layers aimed at minimizing coulombic efficiency losses.

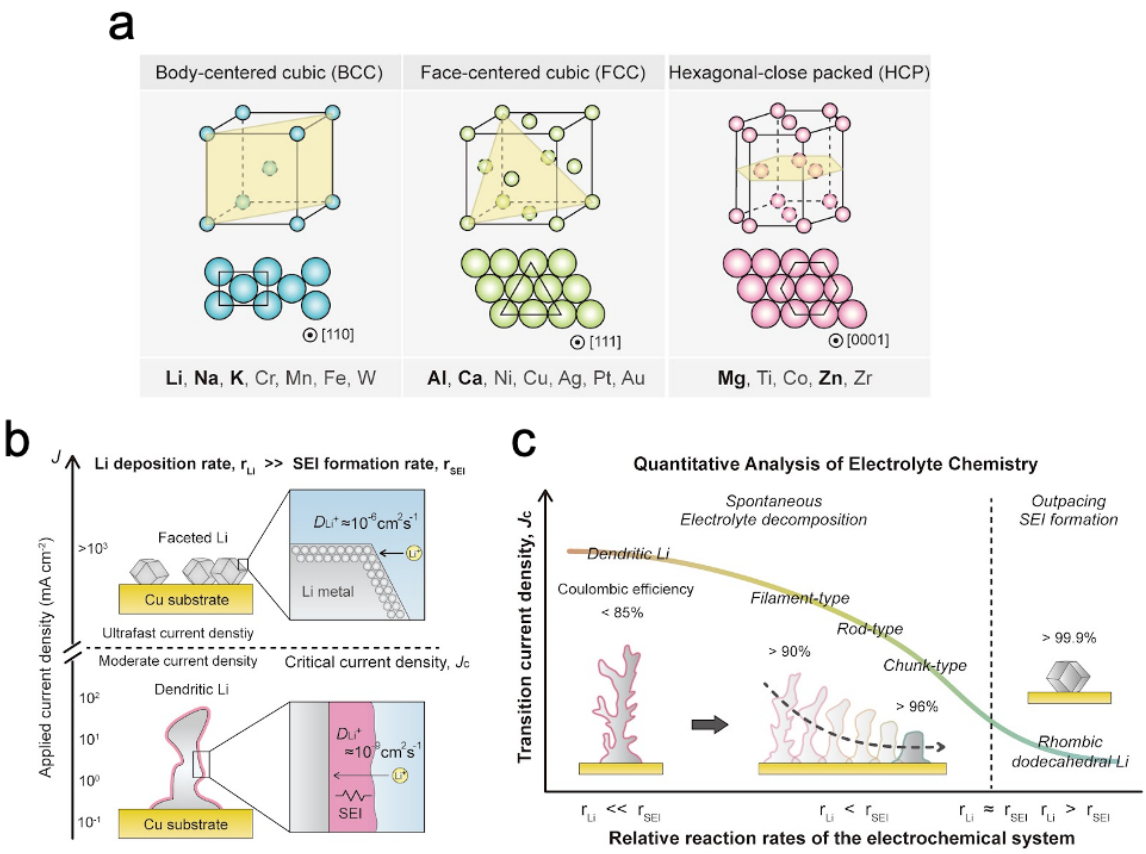


Figure 5. Electrodeposition of reactive metals and quantitative analysis of electrolyte kinetics with microelectrodes.

(a) The morphologies of various polymorphs, consisting solely of a family of close-packed planes.

(b) Scheme for morphological transition of deposited Li, which is dictated by relative kinetics between Li deposition rate and SEI formation rate.

(c) Quantitative analysis of electrolyte kinetics to correlate transition current density with Li morphology.

(3) Correlative in situ Characterization

In situ microscopy techniques, including electrons,[27] X-rays,[28,29] and optical microscopies,[30,31] have advanced significantly, allowing the observation of changes in state-of-charge and other physical properties during battery cycling. However, the microscopic field of view often does not match the size of macroscopic electrodes used for electrochemical cycling. Microelectrodes can bridge this length scale by localizing the electrochemical signature to an area comparable to the microscopic observation field (Figure 6). This approach is particularly practical for in situ optical and potentially X-ray microscopy, which typically image areas in the tens of microns. Developing new electrochemical cells compatible with these techniques could substantially enhance the ability to correlate electrochemical and spectro-microscopic signatures, even enabling the identification of beam-induced radiation damage caused by focused X-rays.

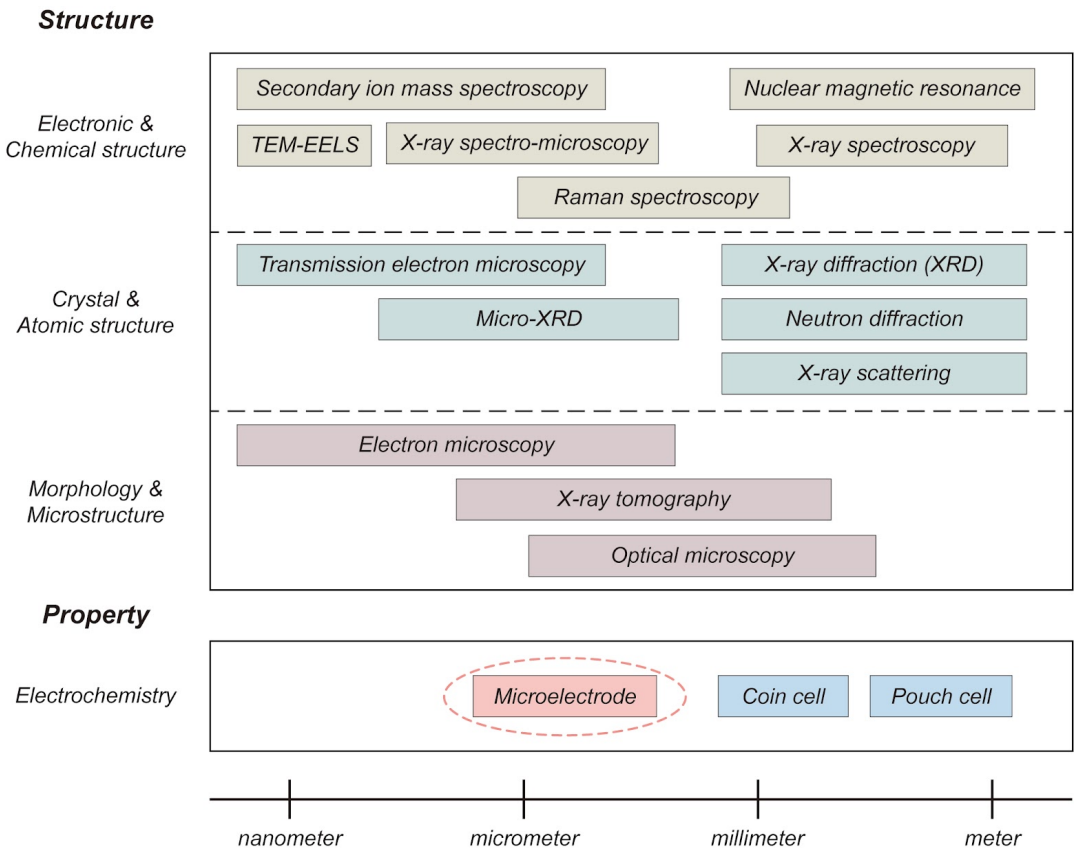


Figure 6. Characterization techniques at multiple length scales (red dotted circle: microelectrode measurements).

(4) High-Throughput and Autonomous Experimentation

Embedding multiple microelectrodes onto a single chip implements high-throughput and autonomous approaches. Multiplexed microelectrode arrays, a commonly used tool in neuroscience research, can significantly speed up sample preparation compared to traditional electrochemical cells.[32] These arrays enable simultaneous measurements with hundreds of electrodes, resulting in expedited faster data collection and analysis. Combining high-volume microelectrodes with postmortem ex-situ characterization, such as scanning electron microscopy (SEM), can further enhance experimental throughput. Autonomous experimentation, as demonstrated by systems such as the Electrolab for redox flow batteries, can be achieved by incorporating these high-throughput capabilities. This allows iterative testing and optimization of customized electrochemical systems.[19]

The prospects for microelectrodes in electrochemical energy storage systems are promising, offering ample opportunities for both fundamental comprehension and technology enhancements. Microelectrodes can manipulate the way reactive metals are deposited, assess electrolyte kinetics in a precise manner, perform in-situ characterization correlatively, and empower high-performing experimentation by utilizing their distinct features. These technological breakthroughs have the potential to revolutionize the field of electrochemical energy storage, resulting in more efficient and stable energy storage systems for next generation.

Chapter 2: Vanadium Oxide Cathodes for Aqueous Zinc Ion Batteries

2.1 Introduction

Lithium-ion batteries (LIBs) presently dominate the electrochemical energy storage market. However, the use of organic electrolytes has restricted their widespread adoption due to growing safety concerns. Rechargeable aqueous batteries with water-based electrolytes offer considerable potential for grid-scale energy storage due to their environmental safety and straightforward installation. Aqueous electrolytes show ionic conductivities that are approximately three orders of magnitude more than those of organic electrolytes, resulting in a major improvement in high-rate capabilities.[33]

Aqueous zinc-ion batteries (AZIBs) are particularly noteworthy because of the remarkable characteristics of Zn anodes. These include their affordability, availability in nature, scalability, low redox potential (–0.76 V vs. SHE), and significant electrochemical stability in water. AZIBs possess the advantage of leveraging multiple-electron transfer processes, resulting in greater volumetric storage capacity (5855 mAh cm^{-3}) in comparison to lithium or sodium-ion batteries.[34] Despite electrolyte advancements achieving reversible two-electron capacity (617 mAh g^{-1}) of MnO_2 in alkaline Zn/MnO_2 batteries, issues with KOH-based electrolytes, such as irreversible by-product formation and zinc dendrite growth, still hinder rechargeability of AZIBs.[35] In this regard, engineering in mild acidic electrolytes (i.e., 2m ZnSO4, pH ~ 4.13) provides a viable solution to improved reversibility of metallic Zn electrodes.

Nonetheless, it is still difficult to create cathode materials that have both a large capacity and cycling stability because of the strong polarization of bivalent Zn^{2+}. Prussian blue analogues

and various forms of manganese oxides deliver restricted capacity and experience rapid capacity fading. Recent studies have focused on layered vanadium oxides with open framework structures, which permit fast and reversible Zn^{2+} intercalation/deintercalation by providing expanded interlayer spacing. Several types of nanostructured vanadium oxides, such as zero-dimensional nanoparticles, one-dimensional nanowires/nanobelts/nanorods, and two-dimensional nanoflakes, have been created as cathodes for AZIBs. The most well-known work from Nazar and colleagues of bilayered $Zn_{0.25}V_2O_5{\cdot}nH_2O$ nanobelts demonstrated a specific capacity of 300 mAh g^{-1} at 50 mA g^{-1}, maintaining 80% capacity in 1000 cycles.[36] The H_2O and Zn co-insertion mechanism proved by varying interlayer distance of $Zn_{0.25}V_2O_5{\cdot}nH_2O$ plays an important role in a remarkably high discharge capacity. Similarly, $NaV_3O_8.1.5H_2O$ nanobelts form Niu and coworkers exhibited a specific capacity of 380 mAh g^{-1} with 82% retention after 1000 cycles.[37] Nevertheless, these cathodes still suffer from structural deterioration as a result of recurring lattice expansion/contraction and stresses caused by the insertion/extraction of Zn^{2+} during the charge/discharge cycles. This ultimately leads to impaired cyclic stability.

This chapter provides a detailed analysis of vanadium oxide cathodes, covering their structural and electrochemical superiorities, current challenges, and optimal strategies to enhance the performance. We explore innovative approaches, such as the synthesis and characterization of a laser-scribed VO_x-rGO heterostructure, which exhibits remarkable pseudocapacitive Zn^{2+} storage and impressive electrochemical performance. Additionally, this chapter examines the calendar life and anti-aging properties of these heterostructures, and discusses future opportunities in cathodic engineering, electrolyte chemistry, and large-scale applications to pave the way for advanced, durable AZIBs.

2.2 Understanding of Structural Superiorities of Vanadium Oxide Cathodes

Vanadium oxide cathodes exhibit several key advantages stemming from their unique structure and electrochemical properties. These advantages include the diversity of valence states and the structural flexibility of V-O coordination polyhedra, which together enhance the performance and stability of AZIBs.

- **Diverse Range of Valence States:** Vanadium atoms have a wide variety of valence states, encompassing oxidation levels from +2 to +5. This broad spectrum allows for the occurrence of multi-electron transfer in redox reactions, which greatly increases the theoretical capacity of vanadium oxide cathodes. Multiple electron participation in the redox process enables more charge storage per unit mass in comparison to typical cathodes that depend on single-electron transfers (such as $LiCoO_2$, $LiFePO_4$, and $LiMn_2O_4$). For instance, the redox couple V^{5+}/V^{4+} or V^{4+}/V^{3+} can be exploited to attain elevated energy densities in AZIBs.[38]
- **Structural Flexibility Of V-O Coordination Polyhedra:** The V-O coordination polyhedra of vanadium exhibit structural plasticity, with the formation of several oxides that include distinct polyhedra arrangements, such as VO_4 tetrahedra and VO_6 octahedra. During Zn^{2+} insertion, the polyhedra can adjust their shapes and orientations to accommodate the Zn ions, while still preserving the overall structure of the crystal.[39] This adaptability ensures the cathode material to maintain stability across numerous charge-discharge cycles, contributing to the cycling performance of AZIBs.
- **Large Spacing Layered Structures:** Many vanadium oxide nanostructures, including V_2O_5 nanobelts[40] and nanotubes,[41] form multiwalled structures with large interlayer spacings. These

layers provide ample room for Zn^{2+} ions to intercalate and deintercalated, which is pivotal for smooth ion transport maintaining and good rate performance of AZIBs.

- **Comparable Ionic Conductivity:** Some vanadium oxide cathodes, including V_2O_3 and V_6O_{13}, exhibit higher ionic conductivity than many transition metal oxides. For example, V_2O_3 is chosen as a high-capacity cathode for AZIBs because it can share an edge with the adjacent octahedron via two common VO_6 octahedra to form a 3D tunnel, which enables electron transfer along the V-V chain and rapid intercalation of cations.[42]

By leveraging the intrinsic structural and electrochemical properties of vanadium oxide cathodes, researchers can design cathodes that offer high capacity, excellent stability, and efficient ion transport, addressing key challenges in the development of advanced AZIBs.

2.3 Current Challenges with Vanadium Oxide Cathodes in AZIBs

Vanadium oxide cathodes are considered attractive materials for AZIBs due to their large theoretical capacities and diverse valence states. However, despite their potential, numerous formidable obstacles impede their actual implementation. This chapter explores the main challenges that vanadium oxide cathodes encounter, analyzing the fundamental mechanics involved and presenting pertinent examples to highlight these problems.

(1) Sluggish Zn^{2+} Transport Kinetics:

Zinc ions in aqueous electrolytes are encompassed by a solvation sheath that is approximately 5.5 Å in diameter. This sheath needs to be released before the ions can integrate into the cathode, resulting in a significant de-solvation penalty. The de-solvation process involves

the disruption of the strong connections between Zn^{2+} ions and the water molecules in their vicinity, causing a substantial increase in energy that hinders the movement of Zn^{2+} ions.[43] Vanadium oxide cathodes generally exhibit inferior electronic conductivity in comparison to metallic conductors due to their semiconducting nature. The scarcity of free electrons in semiconductors hampers the movement of electric current, leading to reduced electron transfer rates and hindering electrochemical reactions as a whole. For example, V_2O_5, despite having a large theoretical capacity, frequently shows inadequate electronic conductivity. This requires the inclusion of conductive additives to improve its performance.[44] Binders, which are usually non-conductive organic polymers, are included to maintain the cohesion of the electrode materials. Although crucial for maintaining mechanical integrity, they can obstruct ion and electron transport channels, hence worsening conductivity problems.

(2) Structural Pulverization and Vanadium Dissolution

The introduction and removal of Zn^{2+} ions trigger periodic expansion and contraction of the lattice structure in vanadium oxide cathodes. The changes in volume caused by phase transitions generate mechanical stress, resulting in the development of cracks and eventual pulverization of electrode materials. This compromises the structural integrity of the electrode and accelerates the degradation process. Vanadium oxide materials have the tendency to react with water, resulting in the progressive dissolution of vanadium ions. Over time, the vanadium ions from the cathode material dissolve into the electrolyte, causing a reduction in active material and a decline in capacity.

(3) Inert By-product Formation on Electrodes

Layered Double Hydroxides (LDH) can be formed on the electrodes through the reaction between hydroxide ions (OH^-) and zinc salts in the electrolyte. The by-products formed when the electrolyte reacts with the electrode surface operate as a barrier, hindering the movement of ions and decreasing the amount of active material that may participate in electrochemical reactions. Protons and dissolved oxygen in the electrolyte can intercalate into the electrode materials, leading to the creation of inert by-products.[45] The presence of these intercalated species can induce alterations in the structure and obstruct the pathways for ion transport, leading to a further deterioration of the electrode's electrochemical stability.

2.4 Enhancing Electrochemical Performance of Vanadium Oxide Cathodes

Material engineering provides effective approaches to enhance the electrochemical performance of vanadium oxide cathodes in AZIBs. This chapter looks into many efficient techniques, such as utilizing pretreatments to achieve mixed valence states of vanadium and manufacturing heterostructures with conductive additives. These methods tackle important obstacles like inhibiting the accumulation of vanadium species, improving electron conductance, and reducing the dissolution of vanadium in aqueous electrolytes.

2.4.1 Mixed Valence States of Vanadium

The combination of various valence states facilitates multi-electron transfer during the redox process of vanadium, hence promoting the intrinsic redox activity, electron conductivity and theoretical capacity of vanadium oxide cathodes. Different methods including controlled thermal

treatment, hydrothermal synthesis, and chemical reduction have been employed to achieve this goal.

- **Hydrothermal Reduction**: Hydrothermal reduction can be regarded as one of the most popular approaches for crystal growth. It involves subjecting vanadium oxides to different time and temperatures under a high vapor pressure, which can create a mixture of V^{4+} and V^{5+} in vanadium oxides. Heating V_2O_5 in a reducing atmosphere (i.e., hydrogen or ammonia gas) within a sealed container can introduce lower valence states, thereby improving electronic conductivity and electrochemical response.[46]
- **Non-hydrothermal synthesis**: During the synthesis of vanadium oxide cathodes, the occurrence of non-stoichiometric VO_x phases, specifically the Magneli phase (between VO_2 and V_2O_5) and Wadsley phase (between V_2O_3 and VO_2) is inevitable. The typical hydrothermal reduction process is greatly affected by the precursors added to obtain the stable phase. Other synthesis methods, namely spin coating,[47] DC magnetron sputtering,[48] and sol-gel synthesis[49] have been explored to achieve a thermodynamically stable oxide state of VO_x for improved redox activity.
- **Pulsed Laser Deposition (PLD)**: PLD is a rising physical vapor deposition (PVD) technique for growing an assortment of structures, including high-quality epitaxial films and nanostructured layers. During PLD, a concentrated laser beam with high energy is directed at a specific target material with the intended composition. The material that is turned into vapor from the target is then placed on a substrate that is positioned opposite the target. This technique requires an environment with extremely low pressure, known as ultrahigh vacuum (UHV), and can precisely deposit a thin film of mixed -valance vanadium without interference from impurities.[50]

2.4.2 Heterostructures/Composite Structures with Conducting Additives

The incorporation of conducting additives such as graphene, carbon nanotubes (CNTs), or conducting polymers in the manufacture of vanadium oxide cathodes has been found to be advantageous in building heterostructures or composite structures. The conductive additives create interconnected networks that improve electronic conductivity and offer more channels for Zn^{2+} ions storage. The network architecture inhibits the accumulation of vanadium species and preserves the structural integrity of the electrode during repeated cycles, resulting in enhanced electrochemical efficiency. Graphene[51] and CNTs[52] provide exceptional electrical conductivity and mechanical strength. The addition of graphene or CNTs to vanadium oxide cathodes can form conductive networks that facilitate rapid electron and ion transport, bringing about better rate capability and cycling durability. Conducting polymers, such as polyaniline (PANI)[53] and polypyrrole (PPy),[54] have the ability to combine with vanadium oxides as composites. These polymers not only give rise to conductivity but also support in flexibility and mechanical stability, thus mitigating the issues associated with structural pulverization.

2.5 Laser-Scribed VO_x-rGO Heterostructure for Ultrafast Zinc-Ion Energy Storage

This chapter centers on the development and assessment of laser-scribed VO_x-reduced graphene oxide (rGO) heterostructure engineered for ultrafast zinc-ion storage. We commence with the synthesis methodology, elucidating the procedures in fabricating this sophisticated material. Here, the utilization of laser scribing induces localized heating, promoting the formation of mixed valence states of VO_x, while leaving the overall structure of material unaffected. We then make a thorough characterization of the as-synthesized materials to highlight the structural and

compositional attributes that link to its superior performance. Th pseudocapacitive Zn^{2+} storage properties are also investigated, which demonstrates the swift and efficient charge storage mechanisms of the VO_x-rGO heterostructure. This is followed by showcasing the overall electrochemical performance. Finally, we examine the calendar life and anti-aging abilities of the heterostructure, emphasizing its potential for long-term applications in high-performance AZIBs.

2.5.1 Synthesis method

Graphite oxide (GO) powders were produced by mixing GO paste (Nanotechnology) and deionized (DI) water in 1:1 vol% ratio. After well mixing, the GO solution was stored inside the freeze dryer for one week to get rid of structural water. In a typical synthesis, 3 mL of DI water was added to disperse 160 mg of freeze-dried GO powders. Two-minute of tip sonication was utilized for fully dispersion of some bulky GO particles (2 seconds on and 2 seconds off at 100% power output). Concurrently, 40 mg of vanadium chloride (VCl_3, Fisher Scientific) was dissolved into 5 mL of DI water and the solution was subjected to bath sonication for 2 hours. After that, the VCl_3 solution was uniformly added to the GO suspension using a syringe pump. The pumping rate of VCl_3 solution was set as 1.5 mL/hour while stirring of GO suspension at the highest speed to ensure thorough mixing. The syringe tip was bent by hand to keep it close to the solution surface during addition. Following this, the resulting mixture was drop-cast onto a prepared graphite paper (Panasonic) at a density of 200 $\mu L\ cm^{-2}$. The graphite paper was first flattened with ethanol and taped down to ensure a smooth surface for drop casting. The cast film was then left to dry overnight inside the fume hood.

On the second day, the dried film underwent laser scribing using a 40 W Full Spectrum Laser Muse 3D Desktop CO_2 Laser Cutter, set at 12% power and 100% speed with a resolution of

500 x 500 DPI. The electrodes were then cut from the film using a 10 mm hole puncher. For conversion of V^{3+} to higher oxidation states, the electrodes were placed in a tube furnace preheated to 60 °C for 1 hour, then ramped up to 300 °C at 2 °C min^{-1}, and held at 300 °C for 1 hour. Post-calcination, the electrodes were weighed using a microbalance and the active material loading was determined to be around 0.9 mg cm^{-2} by the thermogravimetric analysis (TGA).

2.5.2 Materials characterization

Scanning electron microscopy (SEM) images clearly reveal distinctions between the laser-scribed VO_x-rGO heterostructure and the commercial V_2O_5. Figure 7a depicts the VO_x-rGO heterostructure composed of highly exposed rGO sheets with rough surface. The synthesis procedure effectively integrates and disperses nano-VOx particles within the hierarchically porous framework, resulting in uniform embedding. In contrast, commercial V_2O_5 (Figure 7c) exhibits bulky vanadium species that tend to aggregate, leading to reduced active surface area and poor ion diffusion pathways.

Energy-dispersive X-ray spectroscopy (EDS) was performed to determine the elemental composition of the VO_x-rGO heterostructure before and after calcination. As shown in Figure 7b, the EDS spectra confirm the presence of vanadium (V), oxygen (O), and chlorine (Cl) elements in the as-prepared sample. The peak corresponding to chlorine in the "Before calcination" spectrum indicates residual VCl_3 precursor. After calcination, the chlorine peaks diminish significantly, confirming the effective removal of chlorine and conversion of V^{3+} to higher oxidation states of vanadium, as indicated by the prominent vanadium peaks and following X-ray diffraction (XRD) study.

XRD patterns were recorded to analyze the crystalline phases present in the VO_x-rGO heterostructure. Figure 7d displays well-defined diffraction peaks that correspond to orthorhombic V_2O_5 (JCPDS: 00-041-1426) and monoclinic VO_2 (JCPDS: 00-044-0252). The presence of these phases indicates successful formation of a composite structure comprising both V_2O_5 and VO_2. The layered structure of V_2O_5 and the channel-like structure of VO_2 contribute to enhanced electrical conductivity through electron hopping between V^{4+} and V^{5+}, as well as improved ionic conductivity due to the formation of oxygen vacancies within the material.

The detailed characterization of the VO_x-rGO heterostructure through SEM, EDS, and XRD analyses highlights the significant improvements in structural and compositional properties achieved through the synthesis process. The calcination step is essential for removing precursor residues and achieving the desired oxidation states of vanadium. The unique nanostructure of the VO_x-rGO heterostructure, characterized by uniformly distributed nano-VO_x particles on rGO sheets and the presence of mixed vanadium oxides, contributes to its superior electrochemical performance in AZIBs.

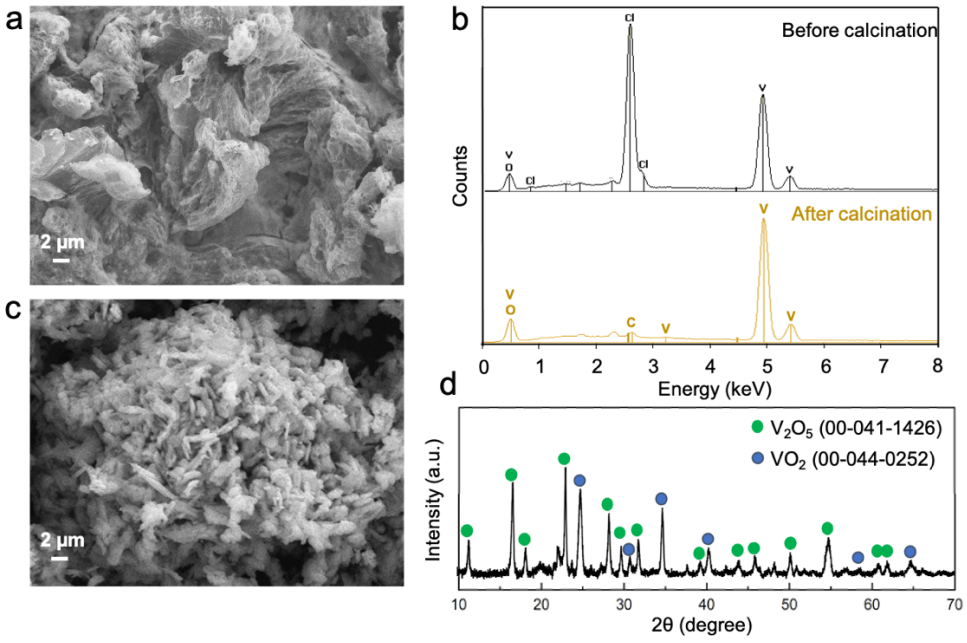


Figure 7. Materials characterization of the laser-scribed VOx-rGO heterostructure.
(a) SEM image of the VO_x-rGO heterostructure showing highly exposed rGO sheets with nano-VO_x particles uniformly embedded in the porous structure. (b) EDS spectra before and after calcination, indicating the removal of chlorine and conversion of V^{3+} to higher oxidation states. (c) SEM image of commercial V_2O_5, showing bulky vanadium species with significant aggregation. (d) XRD patterns of the final VO_x-rGO heterostructure, illustrating the presence of orthorhombic V_2O_5 and monoclinic VO_2 phases.

2.5.3 Pseudocapacitive Zn^{2+} storage

To further investigate the electrochemical kinetics of the VO_x-rGO heterostructure, cyclic voltammetry (CV) curves were recorded within the voltage range of 0.3 to 1.6 V, as shown in Figure 8a. The CV curves display two distinct pairs of redox peaks corresponding to the Zn^{2+} insertion/extraction, indicating the occurrence of reversible Faradaic reactions during the charge transfer process. In the context of pseudocapacitive storage, these reactions can occur both near and on the surface of the electrode material, facilitating rapid charge and discharge cycles. This is distinct from purely capacitive behavior, which involves electrostatic charge storage without electron transfer[55]. The relationship between the peak current (i) and the scan rate (v) of CV curves follows an empirical power-law relationship, given by the equation:

$$i = av^b$$

where a and b are experimentally determined constants. Specifically, a b value of 0.5 signifies a diffusion-controlled process, while a b value approaching to 1.0 indicates a surface-controlled capacitive process.[56]

As illustrated in Figure 8b, the b values for the four redox peaks in our VO_x-rGO heterostructure were found to be 1.025, 1,015, 1.117, and 1.011 across a range of sweep rates from 0.2 to 2 mV s^{-1}. These values, all close to 1, demonstrate that the electrochemical reactions during charge and discharge are predominantly surface-controlled, rather than being limited by diffusion and mass transfer processes. The superior Faradaic pseudocapacitive response of the VO_x-rGO heterostructure is attributed to its unique nanostructure. The current contributions from surface-controlled and diffusion-controlled processes can be deconvoluted using the following equation:

$$i(v) = k_1 v + k_2 v^{1/2}$$

where k_1 and k_2 represent the contributions from surface-controlled and diffusion-controlled processes, respectively. With increasing scan rates, the proportion of surface-controlled charge storage increases. The integrated overall area under the CV curve, Q_f, helps in determining the contributions from both capacitive and diffusion-controlled processes.[57] And can be expressed as:

$$Q_f = \int_0^V (k_1 v + k_2 v^{1/2}) dE = \int_0^V k_1 dE + \int_0^V k_2 dE$$

Specifically, as shown in Figure 7c, the ratio of surface-controlled charge storage for the VO_x-rGO heterostructure increases from 91.97% at 0.2 mV s^{-1} to 94.22% at 1 mV s^{-1}, and reaches 98.93% at 2 mV s^{-1}. These high surface-controlled capacity contributions are among the highest reported for zinc-ion chemistry, indicating that VO_x-rGO heterostructure, typically non-capacitive for vanadium oxides, exhibits a pseudocapacitive nature in this configuration.

The galvanostatic intermittent titration technique (GITT) is applied to probe the diffusion coefficient of Zn^{2+} in the VO_x-rGO heterostructure. The assembled coin-cell is discharged and charged at a current density of 0.2 mA g^{-1} for 10 minutes, followed by a relaxation period of 3 hours to balance the voltage. This procedure is repeated throughout the whole charge-discharge

protocol until the cut-off voltage is reached. Figure 8d shows the Zn^{2+} diffusion coefficients of the VO_x-rGO heterostructure calculated from the GITT curves based on the formula:

$$D_{Zn^{2+}} = \frac{4}{\pi\tau}\left(\frac{m_B V_m}{M_B s}\right)^2\left(\frac{\Delta E_s}{\Delta E_\tau}\right)^2$$

where τ is the relaxation time, m_B is the mass of active materials, V_m is the molar volume of active materials, M_B is the relative molecular weight of active materials, s is the contact area between the electrode and electrolyte, and ΔEs and ΔEτ are the changes of potential caused by pulse current and constant current charge/discharge, respectively.[58] The D_{Zn2+} of the VO_x-rGO heterostructure during the Zn^{2+} insertion/extraction process is around 10^{-5} cm^2/s below 0.9 V and shifts to 10^{-9} cm^2/s beyond that voltage threshold. This diffusion coefficient range is among the best reported for vanadium oxide cathodes in AZIBs. The difference in ion diffusion kinetics between 0.3-0.9 V and above 0.9V corresponds to the two-stage phase transition of the VO_x structure, which will be discussed in the following chapter.

The high b values, significant surface-controlled capacity contributions and enhanced Zn^{2+} diffusivity suggest that the charge storage in the VO_x-rGO film is confined to the cathode surface, occurring through ultrafast pseudocapacitive kinetics. Despite this surface confinement, the charge storage mechanism remains Faradaic, enabling the material to achieve both ultrafast charging and high-capacity Zn^{2+} energy storage.

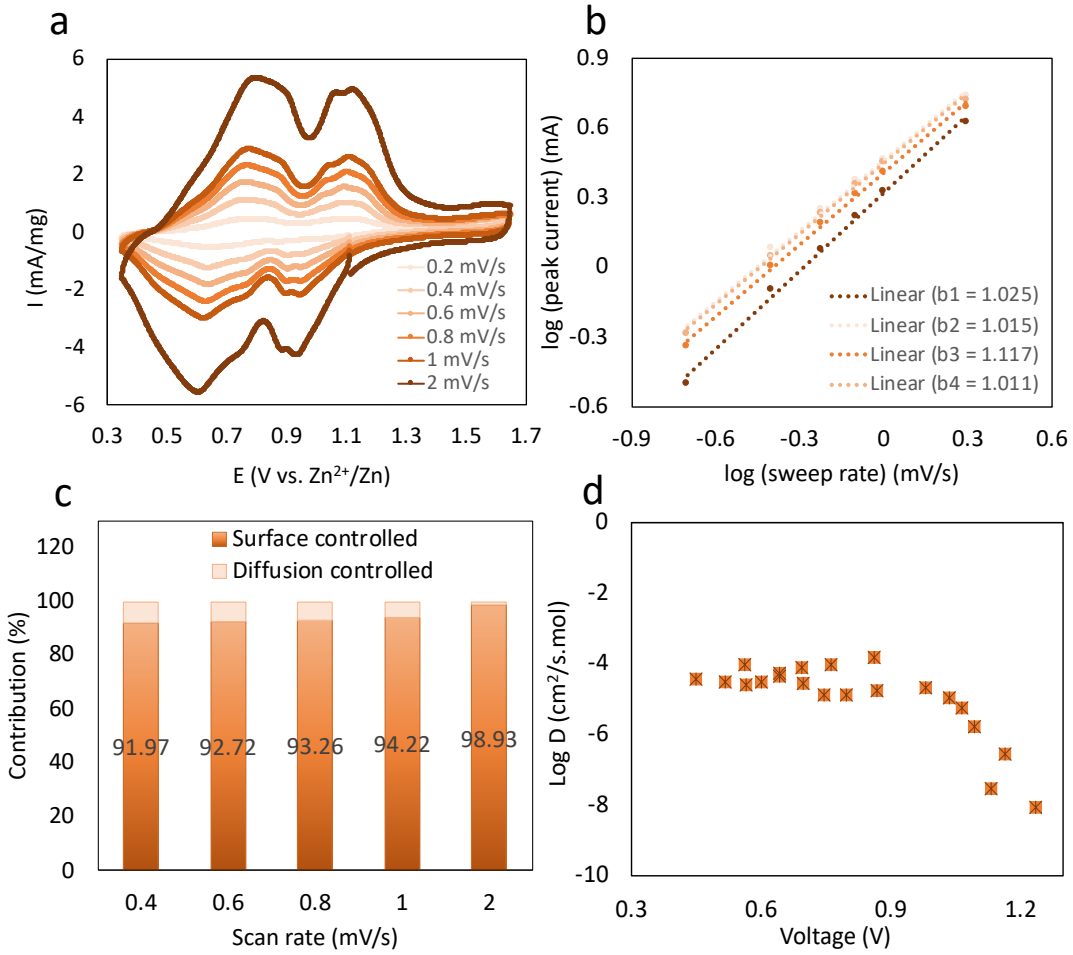


Figure 8. Pseudocapacitive Zn2+ storage of the laser-scribed VOx-rGO heterostructure.

(a) Cyclic voltammetry (CV) curves recorded in the voltage range of 0.3 to 1.6 V, displaying two pairs of redox peaks indicative of reversible Faradaic reactions. (b) Plot of log(i) vs. log(v) for the four redox peaks, showing b values close to 1, suggesting predominantly surface-controlled capacitive processes. (c) Bar graph depicting the contributions of surface-controlled and diffusion-controlled processes to the total capacity at various scan rates. The proportion of surface-controlled charge storage increases with increasing scan rates, reaching 98% at 2 mV s^{-1}. (d) Zn^{2+} diffusion coefficients calculated from GITT curves, showing high diffusion kinetics of VO_x-rGO heterostructure, especially below 0.9 V.

2.5.4 Electrochemical performance

As shown in Figure 9a, the VO_x-rGO heterostructure achieves a high specific capacity of 505 mAh g^{-1} at a current density of 0.2 A g^{-1}. This capacity is among the highest reported to date for ZIB cathode materials. In contrast, commercial V_2O_5 exhibits a negligible capacity of less than 50 mAh g^{-1} under the same condition. The voltage plateau around 0.9 V indicates a two-stage phase transition in the VO_x structure during the charge/discharge cycle, contributing to its high capacity. The proposed electrochemical reactions can be expressed as:

(i) 0.3-0.9V:

$$V_2O_{4.68} + 0.68\ Zn^{2+} + 0.49\ H_3O^+ + 1.85\ e^- \leftrightarrow H_{1.47}Zn_{0.68}V_2O_{5.17}$$

(ii) 0.9-1.6V:

$$H_{1.47}Zn_{0.68}V_2O_{5.17} + 0.72\ Zn^{2+} + 0.35\ H_3O^+ + 1.79\ e^- \leftrightarrow H_{2.52}Zn_{1.40}V_2O_{5.52}$$

It is worth noting that the co-insertion of H_2O molecules with Zn^{2+} ions into the VO_x-rGO heterostructure plays an important role in the overall Zn^{2+} storage capacity. H_2O molecules facilitate the intercalation process by reducing the energy barrier for Zn^{2+} insertion, thus increasing the specific cathode capacity. The H_2O co-insertion also helps to stabilize the structure of the VO_x layers during repeated charge/discharge cycles, reducing the likelihood of structural degradation and maintaining high performance over extended cycling.

The rate performance of the VO_x-rGO heterostructure is summarized in Figure 9b. The current density was increased stepwise from 0.5 to 100 A/g. Impressively, the VO_x-rGO||Zn cell maintains a capacity of around 220 mAh g^{-1} at an ultra-high current density of over 50 A g^{-1} (Figure 9c). Even at a 200-fold increase in current density to 100 A g^{-1}, the cell retains about 74%

of its initial capacity for cathodes with a loading of 0.8 mg cm^{-2} (67% and 50% capacity retention for 1 mg cm^{-2} and 1.26 mg cm^{-2} respectively). This performance allows the cell to be fully charged to 100% state of charge (SOC) within 10 seconds, demonstrating one of the best rate capabilities reported in the literature. The outstanding rate performance is attributed to the synergistic effects of the VO_x-rGO heterostructure, which enhances electronic conductivity, reduces ion diffusion paths, and provides a robust framework that withstands high-rate cycling.

The cycling stability of the VO_x-rGO||Zn full cell at a current density of 30 A g^{-1} is shown in Figure 9d. The cell exhibits an impressive 97.2% capacity retention after 1000 cycles, with an average Coulombic efficiency (CE) of 99.97%. This long-term stability is attributed to the facile strain relaxation upon Zn cycling, shorter diffusion lengths, and faster Zn^{2+} storage mechanism in the VO_x-rGO heterostructure. The robust structural integrity and high electronic conductivity of the VO_x-rGO heterostructure contribute to its remarkable cycling performance, making it a viable candidate for practical AZIB applications.

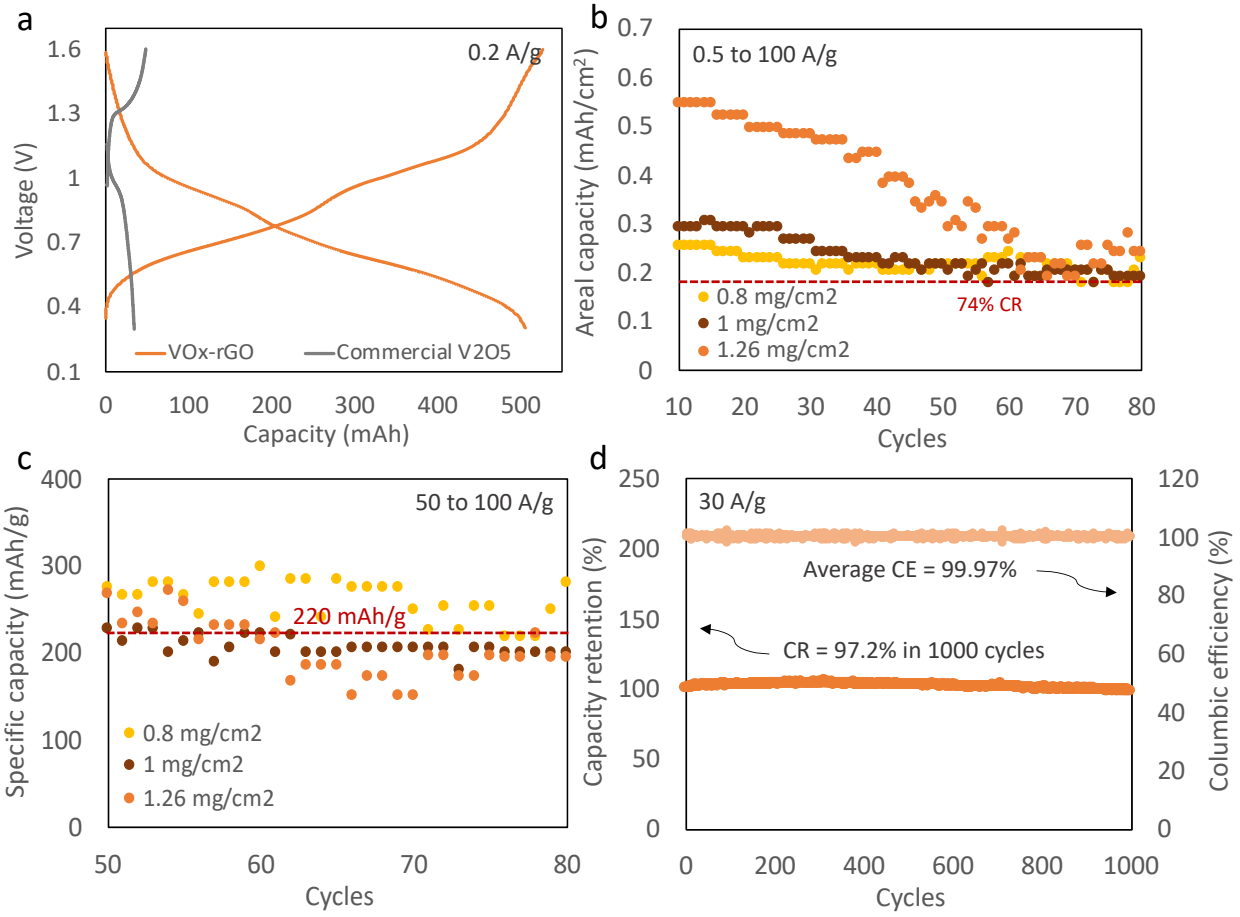


Figure 9. Electrochemical performance of the laser-scribed VOx-rGO heterostructure.

(a) Voltage vs. capacity profile at 0.2 A g^{-1}, showing the high specific capacity (~505 mAh g^{-1}) of VOx-rGO compared to commercial V_2O_5. (b) Areal capacity retention of VOx-rGO from low to high current densities (0.5 to 100 A g^{-1}), maintaining 74% capacity at 100 A g^{-1} for a 0.8 mg cm^{-2} loading. (c) Specific capacity of VOx-rGO at high current densities (50 to 100 A g^{-1}), demonstrating a stable capacity around 220 mAh g^{-1} over multiple cycles. (d) Long-term cycling stability and Coulombic efficiency (CE) of VOx-rGO at 30 A g^{-1}, with 97.2% capacity retention after 1000 cycles and an average CE of 99.97%.

2.5.5 Calendar life and anti-aging ability

Typically, batteries go through long periods of inactivity called calendar aging, during which internal damage occurs due to chemical processes without any current being provided. Despite its significance, calendar aging is frequently disregarded in existing literature. The investigation of performance degradation caused by calendar aging and related mechanisms is still lacking, particularly for AZIBs. There has been a growing recognition of the need for calendar life experiments for LIBs and LMBs. This has brought about systematic examinations of relevant variables, such as states of charge (SOC) and temperatures.

For LMBs, it has been proposed that 50% SOC is a not ideal because the deposited Li is highly porous. This exposes large Li/electrolyte interface area. The optimal storage condition is 0% SOC, or either 100% SOC storage, considering Li anodes have a significantly reduced surface area exposed to the electrolyte. In the case of AZIBs, a significant CE loss of over 15% is observed in merely 12 hours (Figure 10a). Surprisingly, capacity loss can be effectively eliminated when storing at 70% SOC, and almost no capacity loss is observed at an intermediate 50% or lower SOCs during 120 hours of storage. This indicates that storing at a low SOC can reduce unnecessary aging loss and maximize energy efficiency.

To validate if the capacity loss is reversible after aging, normal constant current charge–discharge cycles are proceeded and the ratio of discharge capacity before and after aging is recorded for comparison (table in Figure 10b). After 120 hours of storage, approximately 3.3% of cathodic capacity becomes irreversible, meaning that structural degradation and loss of active sites of cathode materials gradually play a role with extended aging time. Considering the contribution of cathode failure is still minor in the overall CE_{aging}, other factors that lead to varied CE_{aging} in different SOCs are worth exploring.

Replacing H_2O with D_2O and using PVA-based hydrogel shows considerable improvement in CE_{aging} over 24 hours (Figure 10c). The low diffusion coefficient and strong coordination of ions in D_2O can change the bound water in different phases of zinc hydroxide sulfate (ZHS) and potentially retard its generation during aging. The lean-water hydrogel can take the place of the water-rich separator, suppressing the water-induced side reactions and pH variation. Compared to the superior anti-aging ability of LMBs (0.24 ~ 0.42 %/day), over 10% of capacity loss per day is still a big deal and more strategies, including cathodic engineering and electrolyte modification, will be discussed accordingly in the following section.

Moreover, cathodes made with a triple dosage of precursors also demonstrate higher CE_{aging} in different time scales (Figure 10d), which is promising for large-scale and practical applications. Increasing the mass loading of active materials to as high as 10 mg/cm^2 for a target of 3 mAh/cm^2 is expected for a grid-scale utilization of commercial ZIBs. The table in Figure 10d summarizes the mass load of active materials for different precursor dosages, the scalability of this approach can be further boosted with a blade-coating and calendar-pressing method.

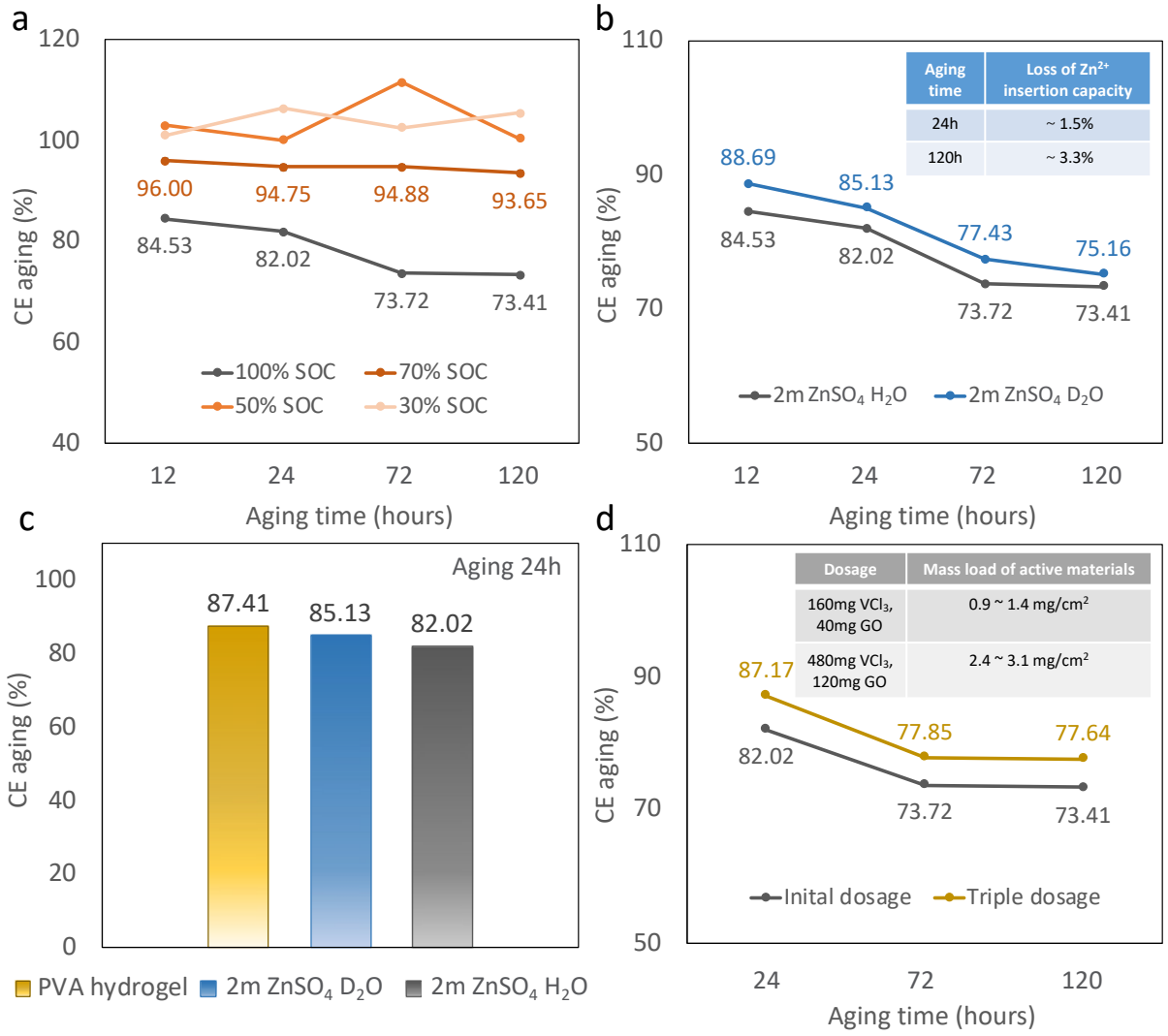


Figure 10. Calendar life and anti-aging ability of the laser-scribed VOx-rGO heterostructure. (a) CE_{aging} of ZIBs at different states of charge (SOC) over 120 hours, showing significant CE loss at 100% SOC, and over 100% of capacity preserved at 50% and 30% SOC. (b) Comparison of CE_{aging} between 2m $ZnSO_4$ in H_2O and D_2O, with a table summarizing Zn^{2+} insertion capacity loss over time. (c) CE_{aging} after 24 hours for different electrolyte compositions, highlighting the benefits of D_2O and PVA hydrogel. (d) CE_{aging} over time for initial and triple dosage of cathode precursors, indicating the potential for large-scale applications.

2.6 Future opportunities

VO_x-rGO heterostructures have demonstrated significant potential in enhancing the performance of AZIBs. This chapter explores future opportunities in three main areas: cathodic engineering, electrolyte chemistry, and large-scale practical applications. By addressing these key aspects, VO_x-rGO heterostructures can be further optimized to meet the demands of next-generation energy storage systems.

2.6.1 Cathodic engineering

(1) Electronic conductivity enhancement

Enhancing electronic conductivity is critical for improving the performance of vanadium oxide cathodes. Our VO_x-rGO heterostructure cathodes provide a good example of combining V-based materials with highly conductive substances. As we discussed in previous chapters, other alternatives including carbon nanotubes and conductive polymers can also be adopted as conductive bridges to facilitate rapid electron transport across the electrode material. Recent reports on constructing 3D conductive frameworks with nickel or graphene foam can provide extensive conductive networks. These frameworks can support the uniform distribution of VO_x nanoparticles and increase the exposure of active sites, which facilitates faster electrochemical reactions and enhances the overall conductivity.

Additionally, mixed valence states of vanadium facilitate high electronic conductivity through electron hopping between different valence states of vanadium, which can be achieved by

a facile laser-scribing process. This simple one-step laser-scribing treatment that can reliably produce porous graphene thin films and simultaneously yield metal oxides at a surface level. The most ideal case is to grow mixed-valance vanadium oxides directly on conductive substrates without the addition of binders. However, it is still challenging to get binder-free cathodes without cracks appearance and curling edge especially at a higher mass loading. In the following chapters, we will discuss the strategies for large-scale application of vanadium oxide cathodes in AZIBs.

(2) Defect engineering

Defect engineering, involving elemental doping and introducing vacancies, is a viable strategy to tune the ionic and electronic conductance of VO_x-rGO heterostructures. Doping vanadium oxides with elements such as Cu, Zn,[59] or Mn[60] can enhance their structural stability and reduce solubility in the electrolyte. These dopants can occupy interstitial sites or substitute for vanadium atoms, strengthening the crystal lattice and reducing the likelihood of dissolution. Oxygen defects[61], in particular, have been introduced to address the strong electrostatic interaction between oxygen atoms and Zn^{2+} ions. Similar to the thermal treatment for mixed-valance VO_x and chemical reduction, methods to introduce oxygen vacancies also include heating VO_x in the reducing atmosphere and adding chemical reducing agents to selectively remove oxygen atoms from the VO_x structure. These oxygen defects motivate local electron enrichment around the defects, significantly improving electronic conductivity and providing additional pathways for ion diffusion. Moreover, this strategy generates a large number of carriers that contribute to ion mobility, resulting in enhanced electrochemical performance.

(3) Surface modification

Surface modification through the construction of a cathode electrolyte interphase (CEI) can mitigate vanadium dissolution. A finest CEI should possess chemical stability in aqueous electrolytes, demonstrate a high level of Zn^{2+} ionic conductivity, be dense enough to prevent direct interaction between the active material and unbound water, be mechanically flexible and strongly adhere to the cathode surface.[45] CEIs can be built through artificial fabrication[62] or in situ reaction.[63] Inorganic coatings,[64, 65] such as graphene quantum dots (GQDs), can alter the electrochemical properties and reduce the dissolution of vanadium during calendaring. While polymer coatings,[66] can be self-sacrificing during cycling, to boost the specific capacity and rate capability of composite cathodes. In this regard, preconstructed CEIs may suffer degradation from repeated volume changes of cathodes, gradually losing their protective function. Contrastively, in situ CEI can continuously regenerate the protective layer, addressing cracks and maintaining its integrity over long-term operations.

2.6.2 Electrolyte chemistry

Optimizing electrolytes for VO_x-rGO heterostructures entails minimizing the presence of active free water and controlling the dissolving equilibrium of active matierals. Water-in-salt electrolytes exemplify this phenomenon, as the elevated concentration of anions hinders the reactions with water molecules, effectively stabilizing the cathode structures.[67] Nevertheless, the viscosity and expense of these electrolytes pose significant obstacles to their industrialization. By including additional solvents like organics, ionic liquids, or deep eutectics,[68-70] with water, it is

possible to mitigate the negative effects of water while maintaining optimum fluidity and high conductivity.

Chemically inhibiting water activity through gel electrolytes and additives is another strategy. Gel electrolytes utilize polymer chains to trap water molecules, while incorporating specialized porosity structures and ion conductors to promote the flow of Zn^{2+} ions, thereby compensating for the absence of water.[71, 72] Additives, such as ethylene glycol, have a strong interaction with water, which can change the way water surrounds and interacts with V-based cathodes as blockers.[73] Some surfactants possess a high affinity for cathodes, can create a hydrophobic coating on cathode surface, providing further protection during battery storage.[74]

Introducing metal salts containing transition metal cations that are identical to those found in the cathodes can influence the rate at which dissolution occurs.[37, 75] The existence of these metal cations can cause a shift in the equilibrium towards reduced dissolution. Sometimes they also contribute to the formation of a robust CEI, offering additional shielding for the cathode materials.

2.6.3 Large-Scale and Practical Applications

A significant challenge for practical applications of AZIBs is the disparity between high-rate and low-rate cycling performance. In past reports, many cathode materials show promising long-term durability under high rates but subpar efficiency under low rates, which are more relevant for the demands of stationary grid storage.[76] The differences in performance suggest that deterioration of cathode materials, either through electrochemical or chemical processes, is less pronounced while operating at high rates. Based on our experimental observation, it has been found that AZIBs can be cycled for a longer duration when operated at a low rate as opposed to a fast rate. This phenomenon is somewhat counter-intuitive.

Additionally, cells with low areal capacities, which are far lower than the realistic values utilized in commercial LIBs, have been frequently reported with impressive rate capability. The low areal capacity of cathode materials highlights the underutilization of Zn anodes. To evaluate AZIBs more realistically, it is essential to provide data on both the specific and volumetric energy density, while also considering the realistic utilization of Zn or the controlled capacity ratios between the negative and positive electrodes (N/P ratios). Using an anode-less cell configuration can provide a more rigorous assessment of energy density. Developing thicker cathodes with higher mass load or new cathode materials with better specific capacities is pivotal for practical applications.

Future opportunities for vanadium oxide cathodes in AZIBs lie in cathodic engineering, electrolyte chemistry, and large-scale practical applications. Enhancing electronic conductivity, defect engineering, and surface modification can significantly improve cathode performance. Optimizing electrolytes by reducing active water and introducing additives can stabilize the structure and enhance conductivity. Addressing challenges related to high C-rates, low areal capacities, and Zn anode utilization is essential for advancing the practical application of AZIBs. By focusing on these areas, vanadium oxide cathodes can play a vital role in developing high-performance, durable AZIBs for various applications.

Reference

1. Zhu, C., Usiskin, R. E., Yu, Y., & Maier, J. (2017). The nanoscale circuitry of battery electrodes. *Science, 358*(6369), eaao2808. https://doi.org/10.1126/science.aao2808
2. Li, Y., & Chueh, W. C. (2018). Electrochemical and chemical insertion for energy transformation and switching. *Annual Review of Materials Research, 48*(1), 137–165. https://doi.org/10.1146/annurev-matsci-070317-124525
3. Wightman, R. M. (1981). Microvoltammetric electrodes. *Analytical Chemistry, 53*(9), 1125A-1134A. https://doi.org/10.1021/ac00232a004
4. Bond, A. M., Fleischmann, M., & Robinson, J. (1984). Electrochemistry in organic solvents without supporting electrolyte using platinum microelectrodes. *Journal of Electroanalytical Chemistry and Interfacial Electrochemistry, 168*(1), 299–312. https://doi.org/10.1016/0368-1874(84)87106-3
5. Anderson, T. J., & Zhang, B. (2016). Single-nanoparticle electrochemistry through immobilization and collision. *Accounts of Chemical Research, 49*(11), 2625–2631. https://doi.org/10.1021/acs.accounts.6b00334
6. Brina, R., Pons, S., & Fleischmann, M. (1988). Ultramicroelectrode sensors and detectors: Considerations of the stability, sensitivity, reproducibility, and mechanism of ion transport in gas phase chromatography and in high performance liquid phase chromatography. *Journal of Electroanalytical Chemistry and Interfacial Electrochemistry, *244*(1), 81–90. https://doi.org/10.1016/0022-0728(88)80096-2
7. Shin, H., Jeong, S., Lee, J., Sun, W., Choi, N., & Cho, I. (2021). 3D high-density microelectrode array with optical stimulation and drug delivery for investigating neural circuit dynamics. Nature Communications, 12(1), 1-18. https://doi.org/10.1038/s41467-020-20763-3

8. Heinze, J. (1993). Ultramicroelectrodes in electrochemistry. *Angewandte Chemie International Edition in English, 32*(9), 1268–1288. https://doi.org/10.1002/anie.199312681
9. Forster, R. J. (1994). Microelectrodes: new dimensions in electrochemistry. *Chemical Society Reviews*, *23*(4), 289. https://doi.org/10.1039/cs9942300289
10. Walsh, D. A., Lovelock, K. R. J., & Licence, P. (2010). Ultramicroelectrode voltammetry and scanning electrochemical microscopy in room-temperature ionic liquid electrolytes. *Chemical Society Reviews, 39*(11), 4185–4194. https://doi.org/10.1039/B822846A
11. Wang, Y., Rogers, E. I., & Compton, R. G. (2010). The measurement of the diffusion coefficients of ferrocene and ferrocenium and their temperature dependence in acetonitrile using double potential step microdisk electrode chronoamperometry. Journal of Electroanalytical Chemistry, 648(1), 15–19. https://doi.org/10.1016/j.jelechem.2010.07.006
12. Li, Y., Zhu, M., Bandari, V. K., Karnaushenko, D. D., Karnaushenko, D., Zhu, F., & Schmidt, O. G. (2022). On-chip batteries for dust-sized computers. *Advanced Energy Materials, 12*(13), 2103641. https://doi.org/10.1002/aenm.202103641
13. Pan, X., Hong, X., Xu, L., Li, Y., Yan, M., & Mai, L. (2019). On-chip micro/nano devices for energy conversion and storage. *Nano Today*. https://doi.org/10.1016/J.NANTOD.2019.100764
14. Xu, C., Li, Q., Wang, Q., Kou, X., Fang, H., & Yang, L. (2021). Femtosecond laser drilled micro-hole arrays in thick and dense 2D nanomaterial electrodes toward high volumetric capacity and rate performance. *Journal of Power Sources, 492*, 229638. https://doi.org/10.1016/J.JPOWSOUR.2021.229638

15. Sur, U. K., Dhason, A., & Lakshminarayanan, V. (2011b). A Simple and Low-Cost Ultramicroelectrode Fabrication and Characterization Method for Undergraduate Students. *Journal of Chemical Education*, *89*(1), 168–172. https://doi.org/10.1021/ed101065e
16. Zhang, H., Xiao, X., Su, T., Gu, X., Jin, T., Du, L., & Tang, J. (2014). A novel thermocouple microelectrode for applications in SECM and variable temperature electrochemistry. *Electrochemistry Communications*, *47*, 71–74. https://doi.org/10.1016/j.elecom.2014.06.027
17. Tanwar, A., Gandhi, H., Kushwaha, D., & Bhattacharya, J. (2022). A review on microelectrode array fabrication techniques and their applications. *Materials Today Chemistry*, *26*, 101153. https://doi.org/10.1016/j.mtchem.2022.101153
18. Beesley, D. J., Semple, J., Krishnan Jagadamma, L., Amassian, A., McLachlan, M. A., Anthopoulos, T. D., & DeMello, J. C. (2014). Sub-15-nm patterning of asymmetric metal electrodes and devices by adhesion lithography. *Nature Communications*, *5*(1), 1-9. https://doi.org/10.1038/ncomms4933
19. Oh, I., Pence, M. A., Lukhanin, N. G., Rodríguez, O., Schroeder, C. M., & Rodríguez-López, J. (2023). The Electrolab: An open-source, modular platform for automated characterization of redox-active electrolytes. *Device, 1*(5), 100103. https://doi.org/10.1016/j.device.2023.100103
20. Min, J., Gubow, L., Hargrave, R., Siegel, J., & Li, Y. (2023). Direct measurements of size-independent lithium diffusion and reaction times in individual polycrystalline battery particles. *Energy & Environmental Science*. https://doi.org/10.1039/D3EE00953J
21. Yuan, X., Liu, B., Mecklenburg, M., & Li, Y. (2023). Ultrafast deposition of faceted lithium polyhedra by outpacing SEI formation. *Nature*, *620*(7972), 86-91. https://doi.org/10.1038/s41586-023-06235-w

22. Munakata, H., Takemura, B., Saito, T., & Kanamura, K. (2012). Evaluation of real performance of LiFePO4 by using single particle technique. *Journal of Power Sources, 217*, 444–448. https://doi.org/10.1016/j.jpowsour.2012.06.037

23. Dokko, K., Nakata, N., Suzuki, Y., & Kanamura, K. (2010). High-rate lithium deintercalation from lithiated graphite single-particle electrode. *Journal of Physical Chemistry C, 114*(18), 8646–8650. https://doi.org/10.1021/jp101166d

24. Dokko, K., Fujita, Y., Mohamedi, M., Umeda, M., Uchida1, I., & Selman1, J. (2001). Electrochemical impedance study of Li-ion insertion into mesocarbon microbead single particle electrode: Part II. Disordered carbon. Electrochimica Acta, 47(6), 933-938. https://doi.org/10.1016/S0013-4686(01)00809-X

25. Dokko, K., Mohamedi, M., Umeda, M., & Uchida, I. (2003). Kinetic Study of Li-Ion Extraction and Insertion at LiMn2O19 Single Particle Electrodes Using Potential Step and Impedance Methods. *Journal of the Electrochemical Society*, *150*(4), A425. https://doi.org/10.1149/1.1556596

26. Dokko, K., Mohamedi, M., Fujita, Y., Itoh, T., Nishizawa, M., Umeda, M., & Uchida, I. (2001). Kinetic Characterization of Single Particles of LiCoO2 by AC Impedance and Potential Step Methods. *Journal of the Electrochemical Society*, *148*(5), A422. https://doi.org/10.1149/1.1359197

27. Yuan, Y., Amine, K., Lu, J., & Shahbazian-Yassar, R. (2017). Understanding materials challenges for rechargeable ion batteries with in situ transmission electron microscopy. *Nature Communications, 8*(1), 15806. https://doi.org/10.1038/ncomms15806

28. Tan, C., Leach, A. S., Heenan, T. M. M., Parks, H., Jervis, R., Weker, J. N., Brett, D. J. L., & Shearing, P. R. (2021). Nanoscale state-of-charge heterogeneities within polycrystalline

nickel-rich layered oxide cathode materials. *Cell Reports Physical Science, 2*(12), 100647. https://doi.org/10.1016/j.xcrp.2021.100647

29. Koo, B., Chung, J., Kim, J., Fraggedakis, D., Seo, S., Nam, C., Lee, D., Han, J., Jo, S., Zhao, H., Nadkarni, N., Wang, J., Kim, N., Weigand, M., Bazant, M. Z., & Lim, J. (2023). Dynamic surface phases controlling asymmetry of high-rate lithiation and delithiation in phase-separating electrodes. *Energy & Environmental Science, 16*(8), 3302–3313. https://doi.org/10.1039/D3EE00341H
30. Merryweather, A. J., Schnedermann, C., Jacquet, Q., Grey, C. P., & Rao, A. (2021). Operando optical tracking of single-particle ion dynamics in batteries. *Nature, 594*(7864), 522–528. https://doi.org/10.1038/s41586-021-03584-2
31. Sharma, N., Vasconcelos, L. S. de, Hassan, S., & Zhao, K. (2022). Asynchronous-to-synchronous transition of Li reactions in solid-solution cathodes. *Nano Letters, 22*(14), 5883–5890. https://doi.org/10.1021/acs.nanolett.2c01818
32. Spira, M. E., & Hai, A. (2013). Multi-electrode array technologies for neuroscience and cardiology. *Nature Nanotechnology, 8*(2), 83–94. https://doi.org/10.1038/nnano.2012.265
33. Zhao, X., Liang, X., Li, Y., Chen, Q., & Chen, M. (2021). Challenges and design strategies for high performance aqueous zinc ion batteries. *Energy Storage Materials*, *42*, 533-569. https://doi.org/10.1016/j.ensm.2021.07.044
34. Zhang, Y., Chen, A., & Sun, J. (2021). Promise and challenge of vanadium-based cathodes for aqueous zinc-ion batteries. *Journal of Energy Chemistry*, *54*, 655-667. https://doi.org/10.1016/j.jechem.2020.06.013

35. Yadav, G. G., Gallaway, J. W., Turney, D. E., Nyce, M., Huang, J., Wei, X., & Banerjee, S. (2017). Regenerable Cu-intercalated MnO2 layered cathode for highly cyclable energy dense batteries. *Nature Communications*, *8*(1), 1-9. https://doi.org/10.1038/ncomms14424

36. Kundu, D., Adams, B. D., Duffort, V., Vajargah, S. H., & Nazar, L. F. (2016). A high-capacity and long-life aqueous rechargeable zinc battery using a metal oxide intercalation cathode. *Nature Energy*, *1*(10), 1-8. https://doi.org/10.1038/nenergy.2016.119

37. Wan, F., Zhang, L., Dai, X., Wang, X., Niu, Z., & Chen, J. (2018). Aqueous rechargeable zinc/sodium vanadate batteries with enhanced performance from simultaneous insertion of dual carriers. *Nature Communications*, *9*(1), 1-11. https://doi.org/10.1038/s41467-018-04060-8

38. Liu, F., Chen, Z., Fang, G. *et al*. V_2O_5 Nanospheres with Mixed Vanadium Valences as High Electrochemically Active Aqueous Zinc-Ion Battery Cathode. *Nano-Micro Lett*. **11**, 25 (2019). https://doi.org/10.1007/s40820-019-0256-2

39. Lv, T., Peng, Y., Zhang, G., Jiang, S., Yang, Z., Yang, S., & Pang, H. (2023). How About Vanadium-Based Compounds as Cathode Materials for Aqueous Zinc Ion Batteries? *Advanced Science*, *10*(12), 2206907. https://doi.org/10.1002/advs.202206907

40. D. Su and G. Wang , Single-Crystalline Bilayered V_2O_5 Nanobelts for High-Capacity Sodium-Ion Batteries, *ACS Nano*, 2013, **7** , 11218 —11226

41. Zhang, K., Gao, G., Sun, W., Liang, X., Liu, Y., & Wu, G. (2018). Large interlayer spacing vanadium oxide nanotubes as cathodes for high performance sodium ion batteries. *RSC Advances*, *8*(39), 22053–22061. https://doi.org/10.1039/c8ra03514h

42. Ding, Y., Peng, Y., Chen, S., Zhang, X., Li, Z., Zhu, L., Mo, L. E., & Hu, L. (2019). Hierarchical Porous Metallic V2O3@C for Advanced Aqueous Zinc-Ion Batteries. *ACS*

Applied Materials & Interfaces, *11*(47), 44109–44117. https://doi.org/10.1021/acsami.9b13729

43. Guo, Y., Jiang, H., Liu, B., Wang, X., Zhang, Y., Sun, J., & Wang, J. (2024). Better engineering layered vanadium oxides for aqueous zinc-ion batteries: Going beyond widening the interlayer spacing. *SmartMat*, *5*(1), e1231. https://doi.org/10.1002/smm2.1231
44. Perera, S. D., Patel, B., Nijem, N., Roodenko, K., Seitz, O., Ferraris, J. P., Chabal, Y. J., & Balkus, K. J. (2011). Vanadium Oxide Nanowire–Carbon Nanotube Binder-Free Flexible Electrodes for Supercapacitors. *Advanced Energy Materials*, *1*(5), 936-945. https://doi.org/10.1002/aenm.201100221
45. Xing, Z., Xu, G., Han, J., Chen, G., Lu, B., Liang, S., & Zhou, J. (2023). Facing the capacity fading of vanadium-based zinc-ion batteries. *Trends in Chemistry*, *5*(5), 380-392. https://doi.org/10.1016/j.trechm.2023.02.008
46. Corr, S. A., Grossman, M., Furman, J. D., Melot, B. C., Cheetham, A. K., Heier, K. R., & Seshadri, R. (2008). Controlled Reduction of Vanadium Oxide Nanoscrolls: Crystal Structure, Morphology, and Electrical Properties. *Chemistry of Materials*, *20*(20), 6396–6404. https://doi.org/10.1021/cm801539f
47. Yamaguchi, I., Manabe, T., Kumagai, T., Kondo, W., & Mizuta, S. (2000). Preparation of epitaxial V2O3 films on C-, A- and R-planes of α-Al2O3 substrates by coating-pyrolysis process. *Thin Solid Films*, *366*(1-2), 294-301. https://doi.org/10.1016/S0040-6090(00)00740-9
48. Corr, S. A., Grossman, M., Furman, J. D., Melot, B. C., Cheetham, A. K., Heier, K. R., & Seshadri, R. (2008). Controlled Reduction of Vanadium Oxide Nanoscrolls: Crystal Structure,

Morphology, and Electrical Properties. *Chemistry of Materials*, *20*(20), 6396–6404. https://doi.org/10.1021/cm801539f

49. Pan, G., Yin, J., Ji, K., Li, X., Cheng, X., Jin, H., & Liu, J. (2017). Synthesis and thermochromic property studies on W doped VO2 films fabricated by sol-gel method. *Scientific Reports*, *7*(1), 1-10. https://doi.org/10.1038/s41598-017-05229-9
50. Lee, S., Meyer, T. L., Park, S., Egami, T., & Lee, H. N. (2014). Growth control of the oxidation state in vanadium oxide thin films. *Applied Physics Letters*, *105*(22). https://doi.org/10.1063/1.4903348
51. Liu, Q., Li, Z., Liu, Y., Zhang, H., Ren, Y., Sun, C., Lu, W., Zhou, Y., Stanciu, L., Stach, E. A., & Xie, J. (2015). Graphene-modified nanostructured vanadium pentoxide hybrids with extraordinary electrochemical performance for Li-ion batteries. *Nature Communications*, *6*(1), 1-10. https://doi.org/10.1038/ncomms7127
52. Boukhalfa, S., Evanoff, K., & Yushin, G. (2012). Atomic layer deposition of vanadium oxide on carbon nanotubes for high-power supercapacitor electrodes. *Energy & Environmental Science*, *5*(5), 6872. https://doi.org/10.1039/c2ee21110f
53. Bai, M. H., Liu, T. Y., Luan, F., Li, Y., & Liu, X. X. (2014). Electrodeposition of vanadium oxide–polyaniline composite nanowire electrodes for high energy density supercapacitors. *Journal of Materials Chemistry. A*, *2*(28), 10882–10888. https://doi.org/10.1039/c3ta15391f
54. Bai, M. H., Bian, L. J., Song, Y., & Liu, X. X. (2014). Electrochemical Codeposition of Vanadium Oxide and Polypyrrole for High-Performance Supercapacitor with High Working Voltage. *ACS Applied Materials & Interfaces*, *6*(15), 12656–12664. https://doi.org/10.1021/am502630g

55. Wei, Q., DeBlock, R. H., Butts, D. M., Choi, C., & Dunn, B. (2020). Pseudocapacitive Vanadium-based Materials toward High-Rate Sodium-Ion Storage. *Energy & Environmental Materials*, *3*(3), 221-234. https://doi.org/10.1002/eem2.12131

56. Wang, J., Polleux, J., Lim, J., & Dunn, B. (2007). Pseudocapacitive Contributions to Electrochemical Energy Storage in TiO2 (Anatase) Nanoparticles. *Journal of Physical Chemistry. C*, *111*(40), 14925–14931. https://doi.org/10.1021/jp074464w

57. Javed, M. S., Han, X., Hu, C., Zhou, M., Huang, Z., Tang, X., & Gu, X. (2016). Tracking Pseudocapacitive Contribution to Superior Energy Storage of MnS Nanoparticles Grown on Carbon Textile. *ACS Applied Materials & Interfaces*, *8*(37), 24621–24628. https://doi.org/10.1021/acsami.6b07924

58. Zhu, Y., & Wang, C. (2010). Galvanostatic Intermittent Titration Technique for Phase-Transformation Electrodes. *Journal of Physical Chemistry. C./Journal of Physical Chemistry. C*, *114*(6), 2830–2841. https://doi.org/10.1021/jp9113333

59. Giorgetti, M., Berrettoni, M., & Smyrl, W. H. (2007). Doped V2O5-Based Cathode Materials: Where Does the Doping Metal Go? An X-ray Absorption Spectroscopy Study. *Chemistry of Materials*, *19*(24), 5991–6000. https://doi.org/10.1021/cm701910c

60. Geng, H., Cheng, M., Wang, B., Yang, Y., Zhang, Y., & Li, C. C. (2019). Electronic Structure Regulation of Layered Vanadium Oxide via Interlayer Doping Strategy toward Superior High-Rate and Low-Temperature Zinc-Ion Batteries. *Advanced Functional Materials*, *30*(6). https://doi.org/10.1002/adfm.201907684

61. Zhu, K., Wei, S., Shou, H., Shen, F., Chen, S., Zhang, P., Wang, C., Cao, Y., Guo, X., Luo, M., Zhang, H., Ye, B., Wu, X., He, L., & Song, L. (2021). Defect engineering on V2O3 cathode

for long-cycling aqueous zinc metal batteries. *Nature Communications*, *12*(1), 1-9. https://doi.org/10.1038/s41467-021-27203-w

62. Zhang, L., Zhang, B., Hu, J., Liu, J., Miao, L., & Jiang, J. (2021). An In Situ Artificial Cathode Electrolyte Interphase Strategy for Suppressing Cathode Dissolution in Aqueous Zinc Ion Batteries. *Small Methods*, *5*(6), 2100094. https://doi.org/10.1002/smtd.202100094
63. Liu, H., Jiang, L., Cao, B., Du, H., Lu, H., Ma, Y., Wang, H., Guo, H., Huang, Q., Xu, B., & Guo, S. (2022). Van der Waals Interaction-Driven Self-Assembly of V2O5 Nanoplates and MXene for High-Performing Zinc-Ion Batteries by Suppressing Vanadium Dissolution. *ACS Nano*, *16*(9), 14539–14548. https://doi.org/10.1021/acsnano.2c04968
64. Saravanakumar, B., Purushothaman, K. K., & Muralidharan, G. (2015). High performance supercapacitor based on carbon coated V2O5 nanorods. *Journal of Electroanalytical Chemistry*, *758*, 111-116. https://doi.org/10.1016/j.jelechem.2015.10.031
65. Chao, D., Zhu, C., Xia, X., Liu, J., Zhang, X., Wang, J., Liang, P., Lin, J., Zhang, H., Shen, Z. X., & Fan, H. J. (2014). Graphene Quantum Dots Coated VO2 Arrays for Highly Durable Electrodes for Li and Na Ion Batteries. *Nano Letters*, *15*(1), 565–573. https://doi.org/10.1021/nl504038s
66. Gittleson, F. S., Hwang, J., Sekol, R. C., & Taylor, A. D. (2013). Polymer coating of vanadium oxide nanowires to improve cathodic capacity in lithium batteries. *Journal of Materials Chemistry. A*, *1*(27), 7979. https://doi.org/10.1039/c3ta11049d
67. Zhang, L., Rodríguez-Pérez, I. A., Jiang, H., Zhang, C., Leonard, D. P., Guo, Q., Wang, W., Han, S., Wang, L., & Ji, X. (2019). ZnCl2 "Water-in-Salt" Electrolyte Transforms the Performance of Vanadium Oxide as a Zn Battery Cathode. *Advanced Functional Materials*, *29*(30), 1902653. https://doi.org/10.1002/adfm.201902653

68. Zhao, H., Fu, Q., Luo, X., Wu, X., Indris, S., Bauer, M., Wang, Y., Ehrenberg, H., Knapp, M., & Wei, Y. (2022). Unraveling a cathode/anode compatible electrolyte for high-performance aqueous rechargeable zinc batteries. *Energy Storage Materials*, *50*, 464-472. https://doi.org/10.1016/j.ensm.2022.05.048

69. Liu, Z., Pulletikurthi, G., & Endres, F. (2016). A Prussian Blue/Zinc Secondary Battery with a Bio-Ionic Liquid–Water Mixture as Electrolyte. *ACS Applied Materials & Interfaces*, *8*(19), 12158–12164. https://doi.org/10.1021/acsami.6b01592

70. Zhao, J., Zhang, J., Yang, W., Chen, B., Zhao, Z., Qiu, H., Dong, S., Zhou, X., Cui, G., & Chen, L. (2019). "Water-in-deep eutectic solvent" electrolytes enable zinc metal anodes for rechargeable aqueous batteries. *Nano Energy*, *57*, 625-634. https://doi.org/10.1016/j.nanoen.2018.12.086

71. Wang, Y., Li, Q., Hong, H., Yang, S., Zhang, R., Wang, X., Jin, X., Xiong, B., Bai, S., & Zhi, C. (2023). Lean-water hydrogel electrolyte for zinc ion batteries. *Nature Communications*, *14*(1), 1-10. https://doi.org/10.1038/s41467-023-39634-8

72. Leng, K., Li, G., Guo, J., Zhang, X., Wang, A., Liu, X., & Luo, J. (2020). A Safe Polyzwitterionic Hydrogel Electrolyte for Long-Life Quasi-Solid State Zinc Metal Batteries. *Advanced Functional Materials*, *30*(23), 2001317. https://doi.org/10.1002/adfm.202001317

73. Wang, N., Yang, Y., Qiu, X., Dong, X., Wang, Y., & Xia, Y. (2020). Stabilized Rechargeable Aqueous Zinc Batteries Using Ethylene Glycol as Water Blocker. *ChemSusChem*, *13*(20), 5556–5564. https://doi.org/10.1002/cssc.202001750

74. Hou, Z., Zhang, X., Li, X., Zhu, Y., Liang, J., & Qian, Y. (2017). Surfactant widens the electrochemical window of an aqueous electrolyte for better rechargeable aqueous sodium/zinc battery. *Journal of Materials Chemistry. A*, *5*(2), 730–738. https://doi.org/10.1039/c6ta08736a

75. Pan, H., Shao, Y., Yan, P., Cheng, Y., Han, K. S., Nie, Z., Wang, C., Yang, J., Li, X., Bhattacharya, P., Mueller, K. T., & Liu, J. (2016). Reversible aqueous zinc/manganese oxide energy storage from conversion reactions. *Nature Energy*, *1*(5), 1-7. https://doi.org/10.1038/nenergy.2016.39

76. Li, C., Jin, S., Archer, L. A., & Nazar, L. F. (2022). Toward practical aqueous zinc-ion batteries for electrochemical energy storage. *Joule*, *6*(8), 1733-1738. https://doi.org/10.1016/j.joule.2022.06.002